

Live-Cell Imaging in *Caenorhabditis elegans* Reveals the Distinct Roles of Dynamin Self-Assembly and Guanosine Triphosphate Hydrolysis in the Removal of Apoptotic Cells

Bin He,^{*†} Xiaomeng Yu,^{*†‡} Moran Margolis,[§] Xianghua Liu,^{*} Xiaohong Leng,^{*||} Yael Etzion,[§] Fei Zheng,^{*} Nan Lu,^{*} Florante A. Quiocho,^{*} Dganit Danino,[§] and Zheng Zhou^{*}

^{*}Verna and Marrs McLean Department of Biochemistry and Molecular Biology, Baylor College of Medicine, Houston, TX 77030; and [§]Department of Biotechnology and Food Engineering, Technion, Haifa 32000, Israel

Submitted June 3, 2009; Revised November 16, 2009; Accepted December 4, 2009
Monitoring Editor: Janet M. Shaw

Dynamins are large GTPases that oligomerize along membranes. Dynamin's membrane fission activity is believed to underlie many of its physiological functions in membrane trafficking. Previously, we reported that DYN-1 (*Caenorhabditis elegans* dynamin) drove the engulfment and degradation of apoptotic cells through promoting the recruitment and fusion of intracellular vesicles to phagocytic cups and phagosomes, an activity distinct from dynamin's well-known membrane fission activity. Here, we have detected the oligomerization of DYN-1 in living *C. elegans* embryos and identified DYN-1 mutations that abolish DYN-1's oligomerization or GTPase activities. Specifically, abolishing self-assembly destroys DYN-1's association with the surfaces of extending pseudopods and maturing phagosomes, whereas inactivating guanosine triphosphate (GTP) binding blocks the dissociation of DYN-1 from these membranes. Abolishing the self-assembly or GTPase activities of DYN-1 leads to common as well as differential phagosomal maturation defects. Whereas both types of mutations cause delays in the transient enrichment of the RAB-5 GTPase to phagosomal surfaces, only the self-assembly mutation but not GTP binding mutation causes failure in recruiting the RAB-7 GTPase to phagosomal surfaces. We propose that during cell corpse removal, dynamin's self-assembly and GTP hydrolysis activities establish a precise dynamic control of DYN-1's transient association to its target membranes and that this control mechanism underlies the dynamic recruitment of downstream effectors to target membranes.

INTRODUCTION

Animal cells undergoing programmed cell death (apoptosis) are engulfed by other cells through phagocytosis and are degraded inside phagosomes. The rapid removal of apoptotic cells is important for tissue remodeling, prevention of tissue injury, and the suppression of inflammatory and autoimmune responses (Savill and Fadok, 2000). During the development of the nematode *Caenorhabditis elegans* hermaphrodites, 131 somatic cells and ~500 germ cells undergo programmed cell death and are swiftly removed by their neighboring cells (Metzstein *et al.*, 1998). Apoptotic cells are easily recognized within living animals under the Nomarski differential interference contrast (DIC) optics as highly refractive, button-like objects that are referred to as "cell corpses" (Sulston and Horvitz, 1977; Sulston *et al.*, 1983). During the removal process, an engulfing cell produces thin

cytoplasmic extensions (pseudopods) to embrace the dying cell, creating a phagocytic cup; the fusion of pseudopods generates a phagosome, inside which the cell corpse is degraded (reviewed in Zhou and Yu, 2008). The extension of pseudopods relies on the incorporation of intracellular vesicles to phagocytic cups, which provide both lipid and protein materials necessary for membrane expansion (Touret *et al.*, 2005). The degradation of apoptotic cells inside phagosomes relies on the process of phagosome maturation, during which a series of intracellular organelles including early endosomes, late endosomes, and lysosomes fuse with phagosomes, delivering digestive enzymes and promoting the acidification of phagosomal lumen (reviewed in Kinchen and Ravichandran, 2008; Zhou and Yu, 2008).

Dynamin is a conserved large GTPase that plays pivotal roles in multiple membrane-related cellular and developmental processes (Hinshaw, 2000; Praefcke and McMahon, 2004). Many lines of evidence suggest that during endocytosis, dynamin acts as a mechanochemical enzyme that drives membrane fission and the release of endocytic vesicles (Hinshaw, 2000; Praefcke and McMahon, 2004; Bashkirov *et al.*, 2008; Pucadyil and Schmid, 2008, and the references therein). In addition, dynamin and dynamin-related proteins also act to promote membrane fusion (Peters *et al.*, 2004; Hoppins and Nunnari, 2009). Dynamin has also been proposed to act as a molecular switch (Sever *et al.*, 1999) or cytoskeleton regulator (Orth and McNiven, 2003). In a ge-

This article was published online ahead of print in *MBC in Press* (<http://www.molbiolcell.org/cgi/doi/10.1091/mbc.E09-05-0440>) on December 16, 2009.

[†] These authors contributed equally to this work.

Present addresses: [‡] Department of Biology, Stanford University, Stanford, CA 94305; ^{||} Department of Molecular Pathology, University of Texas M.D. Anderson Cancer Center, Houston, TX 77054.

Address correspondence to: Zheng Zhou (zhengz@bcm.tmc.edu).

netic screen for mutants that are defective in both embryonic development and cell corpse removal, we identified fourteen recessive, loss-of-function alleles of *dyn-1*, the *C. elegans* dynamin gene (Yu *et al.*, 2006). Our subsequent molecular and cell biological characterizations provided direct evidence that dynamin plays critical roles in phagocytosis and phagosome maturation (Yu *et al.*, 2006, 2008).

Classical dynamins, including *C. elegans* DYN-1, are made up of five domains: an N terminus GTPase domain, a middle domain, a pleckstrin homology (PH) domain, a GTPase effector domain (GED), and a C-terminal proline-rich domain (PRD; Figure 1A). The hydrolysis of GTP is essential for driving membrane fission (reviewed in Hinshaw, 2000). The PH domain targets dynamin to negatively charged lipid membranes (Salim *et al.*, 1996; Zheng *et al.*, 1996). The GED domain was proposed to act as an intramolecular GTPase-activating protein (Sever *et al.*, 1999; Narayanan *et al.*, 2005). The PRD mediates interaction with various Src homology 3-containing proteins that act as functional partners (Schmid *et al.*, 1998; Dawson *et al.*, 2006). The middle domain is a highly conserved domain unique for the dynamin family. This report studies the functions of the middle and GTPase domains in *C. elegans* DYN-1.

The *dyn-1* mutant alleles that we isolated can be separated into two classes: those that bear missense mutations in either the GTPase domain (class I) or the middle domain (class II; Figure 1A). By characterizing GTPase domain mutants, we found that DYN-1 facilitates pseudopod extension and phagosome maturation by promoting the recruitment and fusion of endosomes to phagocytic cups as well as the recruitment and fusion of both endosomes and lysosomes to maturing phagosomes in a GTP-dependent manner (Yu *et al.*, 2006, 2008). Interestingly, this apoptotic cell removal activity of DYN-1 is distinct from its activity in endocytosis, demonstrated by particular *dyn-1* mutant alleles that impair only one but not the other activity (Yu *et al.*, 2006). Similar to DYN-1, human dynamin 2 was proposed to promote phagocytosis through regulating membrane expansion rather than membrane fission (Gold *et al.*, 1999; Di *et al.*, 2003). The function of dynamin in apoptotic cell removal thus suggests a less-characterized activity that promotes membrane fusion, directly or indirectly (Gold *et al.*, 1999; Di *et al.*, 2003; Yu *et al.*, 2006). Specifically, we have found that DYN-1 acts as a mediator in the signaling pathways leading to phagosome maturation—it promotes the recruitment of small GTPase RAB-7, a membrane tethering factor, to phagosomal surfaces, and the synthesis of phosphatidylinositol-3-phosphate [PI(3)P] on phagosomal membranes (Yu *et al.*, 2008). During the removal of apoptotic cells, RAB-7 is essential for the recruitment and fusion of lysosomes to phagosomes (Yu *et al.*, 2008). PI(3)P is another important phagosome maturation molecule acting by attracting downstream effectors to the surface of phagosomes (Vieira *et al.*, 2002). Consistent with this signal transduction role, *C. elegans* DYN-1 and VPS-34, a class III phosphatidylinositol (PI) 3-kinase known to convert PI to PI(3)P, were detected to interact when overexpressed in mammalian cell culture (Kinchen *et al.*, 2008).

A prerequisite for the proper function of DYN-1 is its selective association with its target membranes. The association of DYN-1 to extending pseudopods and nascent phagosomes is necessary for its function in the removal of apoptotic cells (Yu *et al.*, 2006). The recruitment of DYN-1 to pseudopods and nascent phagosomes is dependent on the phagocytic receptor CED-1 and its adaptor protein CED-6 (Yu *et al.*, 2006). Lack of DYN-1 enrichment on phagocytic cups or nascent phagosomes, as a consequence of cell corpse

removal defective (*ced-1* or *ced-6* mutations), causes severe defects in engulfment and degradation of cell corpses (Yu *et al.*, 2006, 2008). However, how the dynamic association of DYN-1 to its target membranes is regulated remains poorly understood.

Dynamins monomers assemble into helical polymers in vitro, either in buffers with low ionic strength or along negatively charged lipids at physiological ionic strength (Hinshaw and Schmid, 1995; Sweitzer and Hinshaw, 1998; Stowell *et al.*, 1999; Danino *et al.*, 2004). Recently, point mutations of residues in the middle domain were found to impair dynamin self-assembly in vitro (Ramachandran *et al.*, 2007). Self-assembly modulates dynamin activity in vitro by enhancing its affinity to lipids and its GTP hydrolysis activity (Warnock *et al.*, 1996; Kavran *et al.*, 1998; Klein *et al.*, 1998; Takei *et al.*, 1998).

Despite its extensive characterization in vitro, whether dynamin undergoes self-assembly along specific membrane regions under physiological condition has not been well demonstrated. Dynamins collar around membrane necks was only observed when its GTP hydrolysis activity was inhibited (Takei *et al.*, 1995). It also remains to be established whether dynamin self-assembly is important for its in vivo function. In addition, given the distinct biochemical properties of dynamins' self-assembly and GTPase activities, it remains to be determined whether these two activities affect similar or different aspects of dynamins' in vivo function.

To answer the above-mentioned questions, we established two novel assays with which we detected DYN-1's oligomerization in vivo. We further found that high-order assembly is essential for DYN-1's function in the removal of apoptotic cells, specifically, for its association with phagosomal membranes. In addition, we found that the dissociation of DYN-1 from phagosomal membranes is GTP dependent. Together, the self-assembly and GTP hydrolysis activities establish a regulatory mechanism for the dynamic association of dynamins with its target membranes, through which dynamins regulate the phagosome association of downstream effectors.

MATERIALS AND METHODS

Mutations, Strains, the Generation of Transgenic Animals, and the Depletion of Maternal dyn-1 Product

C. elegans strains were grown at 20°C as described previously (Brenner, 1974). The N2 Bristol strain was used as the reference wild-type strain. Mutations used are described in Riddle *et al.* (1997), except when noted otherwise: LGV, *unc-76(e911)*; LGX, *dyn-1(en9)*, *dyn-1(en40)* (Yu *et al.*, 2006). Germline transformation was performed as described previously (Jin, 1999), in strains carrying an additional homozygous *unc-76(e911)* mutation, using a plasmid carrying the wild-type *unc-76* genomic DNA (Bloom and Horvitz, 1997) as a coinjection marker. We used a previously established strategy to deplete the maternal *dyn-1* product from homozygous *dyn-1* mutant embryos (Yu *et al.*, 2006). The homozygous mutants were maintained via an extrachromosomal array containing the *dyn-1(+)* genomic DNA. As a result of the rescuing activity of the transgene, the transgenic animals were normal and fertile; however, gene expression is usually repressed in the germline due to germline silencing of repetitive extrachromosomal arrays (Kelly *et al.*, 1997; Yu *et al.*, 2006). Among the progeny of the transgenic animals, we identified those embryos that lost the extrachromosomal array, which presumably inherited reduced amount of maternal *dyn-1(+)* product and do not produced zygotic *dyn-1(+)* product, by tracking embryos that did not carry a monomeric red fluorescent protein coinjection marker.

Plasmid Construction

dyn-1 cDNA (Yu *et al.*, 2006) without the stop codon was inserted into two vectors that contain heat-shock promoters $P_{hsp-16/2}$ and $P_{hsp-16/41}$ (Stringham *et al.*, 1992) as *gfp* fusions to generate $P_{hsp-16/2}$ *dyn-1::gfp* (pBZ51) and $P_{hsp-16/41}$ *dyn-1::gfp* (pBZ52), respectively. To introduce the *en9*(I401F) and *n4039*(G204E) mutations, DNA fragments that contain the corresponding mutations were polymerase chain reaction (PCR)-amplified from lysates generated from homozygous mutant

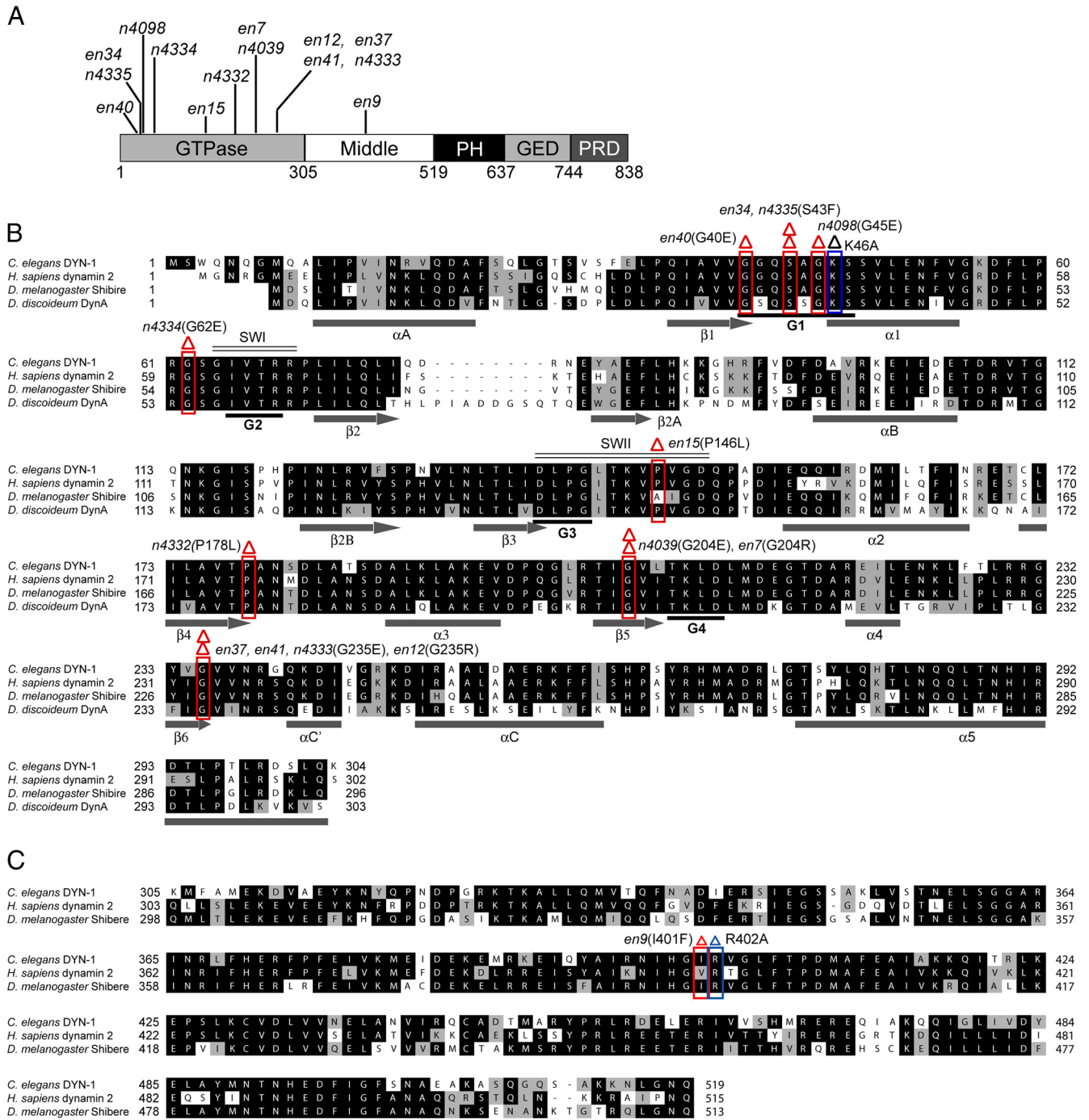


Figure 1. The GTPase and the Middle domains of dynamins in different organisms are highly conserved. (A) Domain structure of DYN-1. The locations of mutations identified from *dyn-1* mutant alleles are indicated. (B and C) GTPase (B) and Middle (C) domain sequence alignment. The residues identical or similar among at least three proteins are shaded in black or gray, respectively. The residues mutated in the *dyn-1* mutant alleles are framed in open red boxes, with the corresponding allele numbers and the amino acid changes indicated above. (B) An open blue box indicates the position of K46A. α -Helices and β -strands identified in DynA are underlined with gray bars and arrows, respectively. G1–G4, highly conserved motifs required for GTP binding and hydrolysis. SWI and II, switch regions I and II. This figure was adapted from figure S2 of Yu *et al.* (2006). (C) An open blue box indicates the position of mutation R402A.

eggs. The SacI-EcoRV fragment that contained the *en9*(I401F) mutation replaced the wild-type fragment, generating $P_{Hsp-16/2} \text{ } dyn-1(I401F)::gfp$ and $P_{Hsp-16/41} \text{ } dyn-1(I401F)::gfp$. The ClaI-NruI fragment that contained the *n4039*(G204E) mutation replaced the wild-type fragment, generating $P_{Hsp-16/2} \text{ } dyn-1(G204E)::gfp$ and $P_{Hsp-16/41} \text{ } dyn-1(G204E)::gfp$. To introduce the *en40*(G40E) and R402A mutations, these mutations were first introduced individually into pBZ51 and pBZ52 by using a site-directed mutagenesis kit (Stratagene, La Jolla, CA) to generate $P_{Hsp-16/2} \text{ } dyn-1(G40E)::gfp$ and $P_{Hsp-16/41} \text{ } dyn-1(G40E)::gfp$ and $P_{Hsp-16/2} \text{ } dyn-1(R402A)::gfp$ and $P_{Hsp-16/41} \text{ } dyn-1(R402A)::gfp$.

The I401F and R402A mutations were further introduced into $P_{Hsp} \text{ } dyn-1(G40E)::gfp$ or $P_{Hsp} \text{ } dyn-1(G204E)::gfp$ plasmids to generate $P_{Hsp} \text{ } dyn-1(G40E \text{ } I401F)::gfp$, $P_{Hsp} \text{ } dyn-1(G204E \text{ } I401F)::gfp$, and $P_{Hsp} \text{ } dyn-1(G40E \text{ } R402A)::gfp$. DNA fragments that contain various mutations were also introduced into $P_{ced-1} \text{ } dyn-1::gfp$ (Yu *et al.*, 2006) to generate $P_{ced-1} \text{ } dyn-1(G40E)::gfp$, $P_{ced-1} \text{ } dyn-1(G204E)::gfp$, and $P_{ced-1} \text{ } dyn-1(I401F)::gfp$. To generate domain truncation mutants, DNA fragments that encode the corresponding DYN-1 protein fragments were cloned into $P_{ced-1} \text{ } dyn-1::gfp$ to make P_{ced-1}

dym-1(GTPase)::gfp, *P_{ced-1} dym-1(ΔPRD)::gfp*, *P_{ced-1} dym-1(ΔGEDΔPRD)::gfp*, *P_{ced-1} dym-1(ΔMD)::gfp*, and *P_{ced-1} dym-1(ΔPH)::gfp*. To construct plasmids for Bimolecular Fluorescence Complementation (BiFC) assays, *dym-1* cDNA were cloned into pCE-BiFC-VN173 and pCE-BiFC-VC155, a pair of BiFC vectors (Shyu *et al.*, 2008), under the control of *P_{hsp-16/41}*, fused, at its C terminus, to cDNAs encoding truncated Venus fragments VN173 (Venus aa 1-173) and VC155 (Venus aa 155-238), respectively, to generate pDYN-1::VN173 and pDYN-1::VC155. The I401F mutation was introduced into the above-mentioned plasmids, respectively, to generate pDYN-1(I401F)::VN173 and pDYN-1(I401F)::VC155. The Middle domain of DYN-1 was deleted from pDYN-1::VN173 and pDYN-1::VC155, respectively, to generate pDYN-1(ΔMD)::VN173 and pDYN-1(ΔMD)::VC155. The *P_{hsp}bFos::VN173* was provided by C.-D. Hu (Purdue University) (Shyu *et al.*, 2008). *P_{ced-1}gfp::rab-5* (pBZ141) was generated by cloning the *rab-5* cDNA, which was PCR amplified from a mixed stage *C. elegans* cDNA library (Z. Zhou and H. R. Horvitz, unpublished data) fusing with *gfp* cDNA that lacked the stop codon to its N terminus under the control of *P_{ced-1}*.

Purification of Recombinant DYN-1 and Rat Dynamin

Wild-type and mutant forms of *C. elegans dym-1* cDNA were cloned into pFast-Bac1 vector (Invitrogen, Carlsbad, CA), and recombinant baculoviruses were generated using the Bac-to-Bac baculovirus expression system (Invitrogen). DYN-1 were expressed in SF21 cells and purified using ammonium sulfate precipitation and Q HP chromatography as described previously (Warnock *et al.*, 1996). The fractions containing DYN-1 were detected by Western blot using anti-rat dynamin 2 antibody (BD Biosciences, San Jose, CA). The purity of the recombinant dynamin is >95% as judged by Coomassie Blue staining. Aliquots with 10% glycerol were quickly frozen in liquid nitrogen and stored at -80°C . Rat dynamin was purified from frozen rat brains (a gift from D. Sackett, National Institutes of Health) following previously described protocol (Stowell *et al.*, 1999).

Antibodies and Western Blots

Polyclonal rabbit antisera against DYN-1 were generated using *Escherichia coli*-expressed recombinant His-tagged full-length DYN-1 as an antigen. Antibodies were affinity purified using the original antigen.

Wild-type strain N2 and different transgenic worms were harvested and boiled in SDS sample buffer (10% sucrose, 2% SDS, 0.0625 M Tris-HCl, pH 6.8, 0.0004% bromophenol blue, and 5% β -mercaptoethanol). Proteins in the supernatants were collected after centrifuge, separated by SDS-polyacrylamide gel electrophoresis (PAGE), and transferred to polyvinylidene difluoride membrane. For detecting DYN-1 and different mutant forms of DYN-1, anti-DYN-1 polyclonal antibody was incubated at a 1:2000 dilution. For detecting green fluorescent protein (GFP)-fused transgenic proteins, monoclonal anti-GFP antibody (Epitomics, Burlingame, CA) was used at a 1:2000 dilution. As the loading control, the same membranes were probed with polyclonal anti-beta-tubulin antibodies (Epitomics).

GTP Binding Assay

A filter assay was used to examine the GTP binding ability of wild-type and mutant dynamin (Song *et al.*, 2004). DYN-1 proteins (0.25 μM) purified from SF21 insect cells (see above) were incubated with 2.5 μM guanosine 5'-O-(3-thio)triphosphate (GTP γS) containing 0.675 $\mu\text{Ci/ml}$ [^{35}S]GTP γS (GE Healthcare, Little Chalfont, Buckinghamshire, United Kingdom) in GTP binding buffer (20 mM HEPES, pH 8.0, 25 mM NaCl, 0.1 mM EGTA, 1 mM MgCl_2 , and 1 mM dithiothreitol) and incubated at room temperature for 20 min in a volume of 60 μl . Each reaction was applied equally to two prewet nitrocellulose filters (Millipore, Billerica, MA) in a filter dot blot apparatus under vacuum (1225 sampling manifold; Millipore) and were subsequently washed with 5 ml of cold GTP binding buffer three times under vacuum. The radioactivity on the filters was measured by liquid scintillation counting. The amount of GTP bound to each sample was measured as cpm and was corrected by subtracting the cpm reading of a no-protein control. Values for each mutant DYN-1 protein were normalized to that of wild-type DYN-1.

Liposome Preparation and Dynamin-Lipid Tube Production

Lipids (phosphatidylserine or total brain lipid; Avanti Polar Lipids, Alabaster, AL) solubilized in chloroform were dried in a glass tube by passing nitrogen gas and kept under vacuum overnight. Hydration of the dry lipid film was accomplished by addition of working buffer (HEPES buffer: 20 mM HEPES-NaOH, pH 7.2, 1 mM MgCl_2 , 2 mM EGTA, and 150 mM NaCl) to the tube to a final concentration of 1 mg/ml, followed by subsequent agitation.

To achieve a homogenous distribution of vesicles, the lipid solution was extruded using a Mini-Extruder (Avanti Polar Lipids) through a polycarbonate membrane (GE Osmonics, Minnetonka, MN). Extrusion through filters with 0.2- μm pores for 13 times yields large, unilamellar vesicles (LUVs) with a mean diameter of 220–240 nm.

Lipid tubes were generated by incubating dynamin samples (0.25 mg/ml) with 200 μM liposomes (0.2 mg/ml) for 2.5 h at room temperature. To test the effect of GTP on the DYN-1-lipid tubes, a drop of dynamin-lipid sample was placed onto the transmission electron microscopy (TEM) grid, GTP was

added in excess (1 mM), followed by an immediate quenching to limit the contact time between the protein complexes and GTP to only 7–14 s.

Electron Microscopy

To ensure microstructural preservation during specimen preparation, vitrified specimens were prepared in the controlled environment vitrification system, a closed chamber enabling sample preparation at well controlled temperatures and at 100% relative humidity. Experiments were done at 25°C . Specimens were prepared by placing a 5- to 8- μl drop of the sample onto a perforated carbon film supported on a TEM copper grid held by tweezers. The drop was then thinned (blotted) by a piece of filter paper wrapped on a thin metal strip to produce a thin specimen film. After blotting the specimen was plunged into liquid ethane at its freezing point (-183°C) and vitrified. The vitrified specimens were stored under liquid nitrogen (-196°C) until observation. In some experiments where contact times between GTP and dynamin-lipid tubes of only few seconds were required, on-the-grid processing was applied (Konikoff *et al.*, 2000; Danino *et al.*, 2004), by adding GTP to the sample on the grid (to a final concentration of 1 mM), followed by immediate blotting and vitrification.

Specimens were examined in a Philips CM120 TEM operated at an accelerating voltage of 120 kV, with an Oxford CT3500 cryo-specimen holder that maintained the vitrified specimens below -175°C . Images at nominal magnifications up to 175K times were recorded digitally by a MultiScan 791 charge-coupled device camera (Gatan, Pleasanton, CA) using the Digital Micrograph 3.4 software package, under low-dose operation to minimize electron beam radiation damage (Danino *et al.*, 2001).

GTP Hydrolysis Assay

GTPase activity was assayed as described previously (Collins and Vallee, 1986; Szafer *et al.*, 2001), with some modifications. Two to 5 g of activated charcoal (Sigma-Aldrich, St. Louis, MO) was weighed and washed three times in distilled water followed by one time of wash in 0.1 M NaH_2PO_4 . Charcoal was divided into Eppendorf tubes containing 600 μl of 0.1 M NaH_2PO_4 , so that each tube contained 5–10% charcoal (wt/vol). 10 mM [γ - ^{32}P]GTP (6000 Ci/mmol; PerkinElmer Life and Analytical Sciences, Boston, MA) was diluted in 10 mM GTP (Sigma-Aldrich) in a 1:20–40 ratio. [γ - ^{32}P]GTP/GTP was added to dynamin or dynamin-decorated lipid tubes in buffer containing 150 mM NaCl to a final concentration of 1 mM and mixed well. Immediately after GTP addition and at each time point measured, 3 μl from the reaction tube was taken into an Eppendorf containing charcoal, 0.1 M NaH_2PO_4 to adsorb organic material, and the reaction was stopped by incubation on ice. Samples were centrifuged in an Eppendorf microcentrifuge for 5 min at maximal speed. Radiation due to free ^{32}P in the supernatant was assayed by scintillation counting to determine the amount of P_i released during the reaction. Maximum radiation was measured by adding 1 mM GTP γ 32 /GTP to 750 μl of 0.1 M NaH_2PO_4 in the absence of charcoal. GTPase activity was represented as the percentage of GTP hydrolyzed, which was calculated as the ratio between the cpm measured at each time point and the maximal radiation.

Quantitation of Cell Corpse Removal Defects by Using DIC Microscopy

The defect in the removal of cell corpses was measured as the number of cell corpses remaining in the body of late fourfold stage embryos using Nomarski DIC microscopy, as described previously (Lu *et al.*, 2009). Late fourfold stage embryos whose bodies made at least three turns and contained a fully developed pharyngeal grinder were scored (Yu *et al.*, 2006).

Heat-Shock Treatment for Inducing the Dominant-Negative Effect of DYN-1 Mutations

Adult hermaphrodites that were 24 h post-larval stage (L4) were allowed to lay eggs for 1 h at 20°C before removed from the plate, which was immediately placed at 30°C for 1 h. The plate was then incubated at 25°C until the embryos on the plate were scored for the number of cell corpses under the DIC optics 8 h later.

BiFC Analyses

BiFC assays were performed using the protocol described in Hiatt *et al.* (2008) and Shyu *et al.* (2008). Transgenic animals carrying pairs of BiFC constructs were raised at 20°C . Embryos on the plate were heat-shocked at 33°C for 1 h. Fluorescent images were captured under the DeltaVision microscope (Applied Precision, Issaquah, WA) 3 h afterward. Serial z-sections in 1- μm interval spanning the entire embryos were captured for each sample. Images were deconvolved and analyzed using SoftWorX software (Applied Precision).

Fluorescence Microscopy and Time-Lapse Recording

An IX70 (Olympus, Tokyo, Japan)-DeltaVision (Applied Precision) microscope equipped with a CoolSNAP digital camera (Photometrics, Tucson, AZ), was used to capture fluorescence images, and SoftWorX software (Applied Precision) was used for image deconvolution and processing (Yu *et al.*, 2008).

Genotype	Overexpression constructs	# cell corpses	Rescue activity
Wild-type	no transgene -	0.3 ± 0.4	-
<i>dyn-1</i> (<i>n4039</i>)	no transgene -	24.4 ± 3.2	0%
	full-length 1 305 519 637 744 838	3.1 ± 1.8	87%
	ΔPRD 1 756	12.1 ± 5.8	51%
	ΔPRDΔGED 1 620	25.5 ± 3.1	0%
	GTPase only 1 317	24.5 ± 4.9	0%
	ΔMD 1 624	23.3 ± 4.1	5%
	ΔPH 1 720	24.5 ± 5.7	0%
	DYN-1(I401F) 1 838	26.4 ± 3.3	0%
	DYN-1(R402A) 1 838	25.0 ± 4.9	0%

Figure 2. The cell corpse removal activities of truncated and mutated DYN-1. The number of cell corpses in late fourfold stage *dyn-1(n4039)* homozygous embryos [progeny of *dyn-1(n4039)/+* mothers] that expressed *dyn-1* cDNAs bearing domain deletions or point mutations under *P_{ced-1}* control are indicated by the diagrams. Data are presented as mean ± SD. For each sample, at least 10 embryos were scored. %Rescuing activity = 100% × (24.4 – mean no. of cell corpses in embryos expressing a particular transgene)/(24.4–0.3). Percentage of rescuing activity is defined as 0 if the number is negative.

To monitor the kinetics of the subcellular localization of various GFP reporters during the engulfment and degradation of cell corpses C1, C2, and C3, the procedure followed an established protocol (Yu *et al.*, 2008; Lu *et al.*, 2009). Recording of the ventral surface of embryos started at 310–320 min post-first cleavage and lasted for 90–120 min in 1- or 2-min intervals. At each time point, 14 serial z-sections at a 0.5-μm interval were recorded. Signs such as embryo elongation and movement were closely monitored to ensure that the embryo being recorded developed normally.

Quantitative Image Analyses

Fluorescence signal intensity was measured and images were analyzed using the ImageJ software (National Institutes of Health, Bethesda, MD) Lu *et al.*, 2009). To calculate the ratio of signal intensity on the surface of phagosomes versus that in the engulfing cell cytosol, the phagosomal surface and cytoplasm were individually defined using the “Free Hand” tool, and the mean value of each selected area was used in the ratio calculation. The enrichment of fluorescence signal on the phagosomal surface was considered significant when the ratio was >1.2.

RESULTS

The GTPase and Middle Domains Are Both Essential for DYN-1’s Function in Cell Corpse Removal

Four *dyn-1* alleles, *en40*, *en34*, *n4335*, and *n4098*, represent changes of three absolutely conserved residues within the G1 motif known for binding the phosphates of guanine nucleotides, and display strong Ced phenotype (Figure 1B; Yu *et al.*, 2006). Mutations *n4334*(G62E) and *en15*(P146L) are adjacent to Switch I and inside the Switch II regions, two regions that undergo major conformational changes between the GDP and GTP-bound states, respectively, and presumably also affect GTP binding or the conformational changes induced by the binding of GTP (Figure 1B). In addition, mutations *n4332*(P178L), *en7*(G204R), *n4039*(G204E), *n4333*, *en37*, *en41*(G235E), and *en12*(G235R) are located in the β4, β5, and β6 strands of the conserved G domain core motif closely

resembling that of Ras GTPase (Figure 1B; Niemann *et al.*, 2001). This group of mutations may induce structural changes of the corresponding β-strands, and subsequently affect GTP binding, hydrolysis, or the interaction of the GTPase domain with other domains. The clustering of such a large number of mutant alleles in the important motifs inside the GTPase domain underscores the importance of GTP hydrolysis for DYN-1 function during cell corpse removal.

To examine the importance of other domains of DYN-1 for the removal of apoptotic cells, we generated extrachromosomal arrays that expressed *dyn-1* cDNA constructs bearing various deletions as *gfp* fusions under the control of the *ced-1* promoter in the *dyn-1(n4039)* mutant worms and scored their activities in rescuing the Ced phenotype (Figure 2). In comparison to the full-length *dyn-1* cDNA, which displayed 87% rescuing activity, deletions of the middle domain or the PH domain alone resulted in complete loss of the rescuing activity (Figure 2), yet did not result in significant changes in the level of the GFP fusion proteins (Supplemental Figure S1, A and C), indicating that the middle and PH domains are both essential for DYN-1’s function in cell corpse removal. The deletion of the GED and PRD domains together also led to a complete loss of rescuing activity (Figure 2). However, this loss could be caused by complex reasons, which include an apparent greatly reduced protein level (Supplemental Figure S1C).

In contrast, removing the PRD domain alone only led to a partial loss of the rescuing activity (Figure 2 and Supplemental Figure S1A), indicating that this domain does not play an essential role in cell corpse removal. We focus on studying the functions of the GTPase and the middle domains in this report.

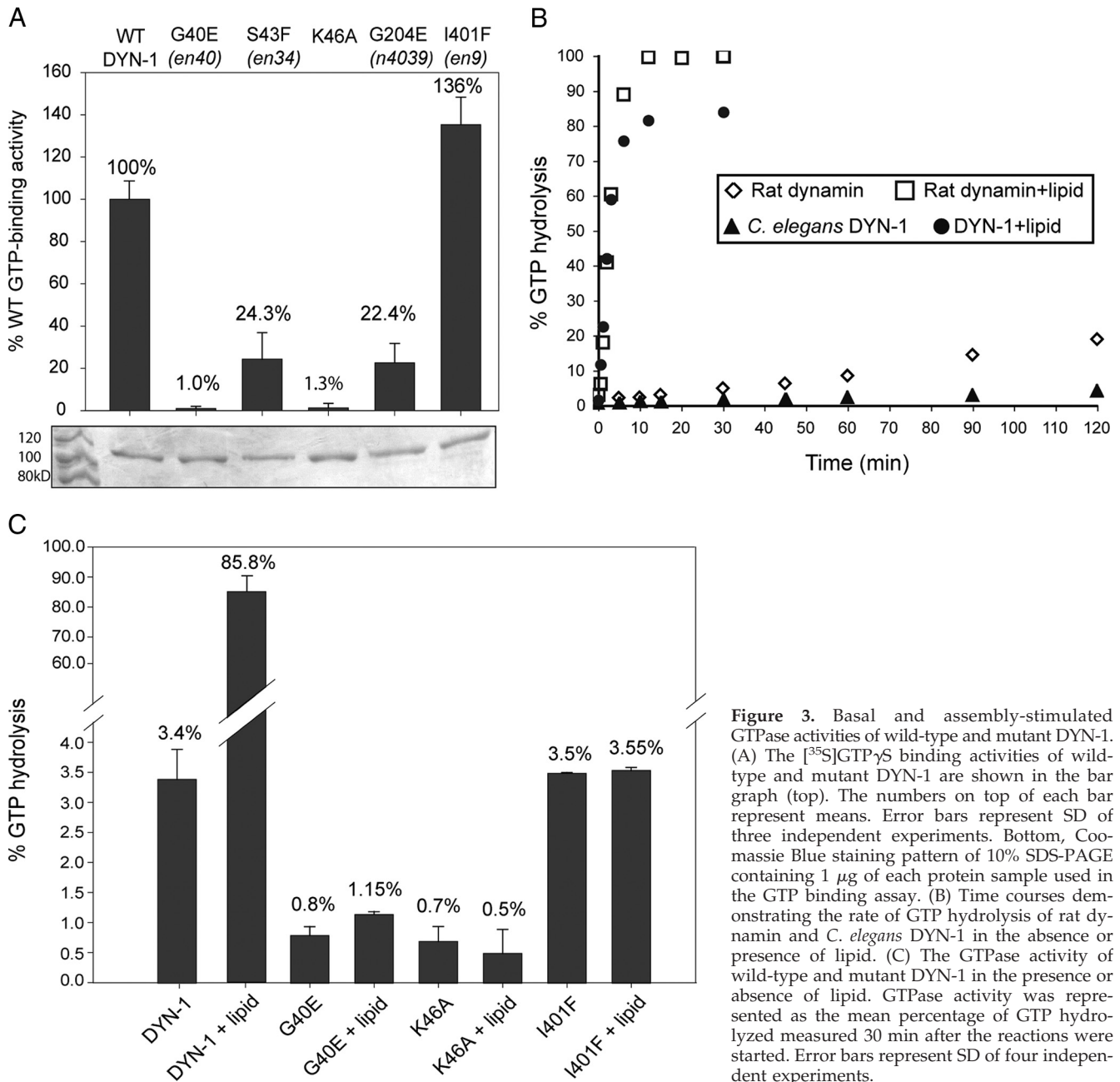


Figure 3. Basal and assembly-stimulated GTPase activities of wild-type and mutant DYN-1. (A) The [35 S]GTP γ S binding activities of wild-type and mutant DYN-1 are shown in the bar graph (top). The numbers on top of each bar represent means. Error bars represent SD of three independent experiments. Bottom, Coomassie Blue staining pattern of 10% SDS-PAGE containing 1 μ g of each protein sample used in the GTP binding assay. (B) Time courses demonstrating the rate of GTP hydrolysis of rat dynamin and *C. elegans* DYN-1 in the absence or presence of lipid. (C) The GTPase activity of wild-type and mutant DYN-1 in the presence or absence of lipid. GTPase activity was represented as the mean percentage of GTP hydrolyzed measured 30 min after the reactions were started. Error bars represent SD of four independent experiments.

Mutations in the GTPase but Not the Middle Domain Affect the GTP Binding Activity of DYN-1

To determine what aspects of DYN-1's biochemical activities are affected by the mutations in the GTPase domain or the middle domain, we expressed wild-type and mutant forms of *dyn-1* cDNAs in an insect cell expression system and purified DYN-1 proteins (Figure 3A) for all the in vitro assays described below. We performed GTP binding assays by measuring the incorporation of [35 S]GTP γ S into DYN-1. In addition to the representative GTPase domain mutations that we identified (Figure 1B), we also analyzed the effect of a K46A mutation, which is equivalent to K44A, a GTP binding-defective mutation in human dynamin 2 (Figure 1B). We found that the G40E and K46A mutations almost abolished the GTP binding activity of DYN-1, whereas the mutations S43F and G204E each reduces the GTP binding activity of

DYN-1 to ~20% of the wild-type level (Figure 3A). In contrast, the I401F mutation did not affect the GTP binding activity of DYN-1 (Figure 3A). These results, together with the strong *Ced* and *embryonic lethal* (*Emb*) phenotypes observed from the corresponding homozygous mutants (see Figure 8A; Yu *et al.*, 2006), indicate that GTP binding is necessary yet not sufficient for DYN-1's in vivo function.

The Middle Domain Mutation I401F Abolishes DYN-1's Assembly-stimulated GTPase Activity

We first examined the GTP hydrolysis activity of DYN-1 mutant proteins in a buffer of physiological ionic strength and inhibitory of dynamin self-assembly (see *Materials and Methods*) (Warnock *et al.*, 1996). By measuring its GTP hydrolysis activity over time, we found that *C. elegans* DYN-1 displayed a low basal-level GTP hydrolysis activity as rat

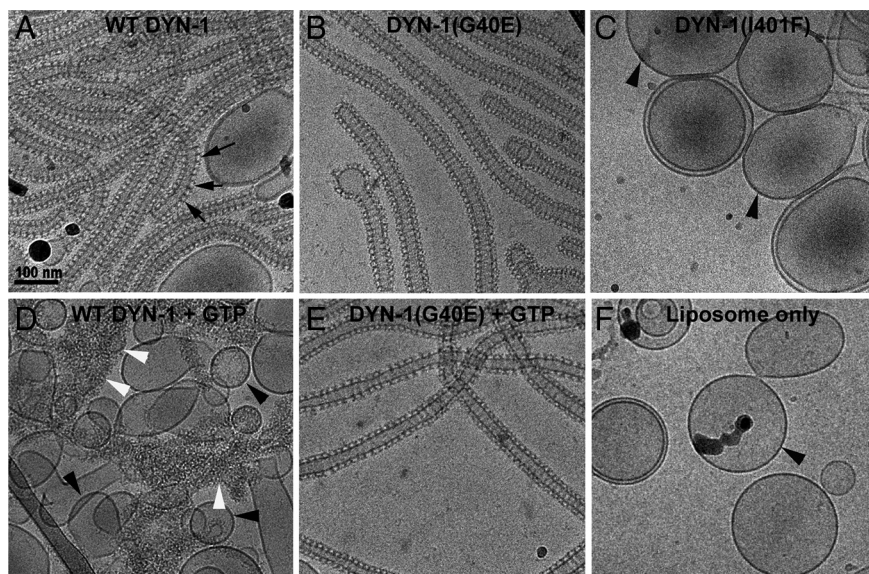


Figure 4. The I401F mutation abolishes DYN-1's ability to assemble along lipid surface. (A–C) Cryo-TEM images of wild-type and mutant DYN-1 incubated with PS liposomes. Wild-type DYN-1 and DYN-1(G40E) both bind to the liposomes and form a protein-coated lipid tubes with defined diameter of ~50 nm. Arrows in A indicate the helical assembly of DYN-1 on lipid tubes. DYN-1(I401F) fails to assemble on the liposome surface (C). (D and E) Cryo-TEM images of DYN-1-lipid (D) and DYN-1(G40E)-lipid samples (E) 7 and 12 s after the addition of 1 mM GTP to the grid containing the dynamin-lipid tubes, respectively. Black arrowheads indicate bare liposomes without DYN-1 coating. White arrowheads in D indicate twisted, constricted dynamin-lipid complexes, which are intermediates of the DYN-1 dissociation process. (F) Cryo-EM image of liposomes (black arrowheads) in the absence of DYN-1 or GTP.

dynamin did (Figure 3B). As expected for mutant DYN-1 molecules that are severely defective for GTP binding, DYN-1(G40E) and DYN-1(K46A) displayed greatly reduced GTP hydrolysis activities in comparison with wild-type DYN-1 (Figure 3C). In contrast, the basal-level GTP hydrolysis activity of DYN-1(I401F) was similar to that of wild-type DYN-1, indicating that the intrinsic GTPase function of DYN-1 was not altered by this mutation (Figure 3C).

In vitro, dynamin oligomerization (or self-assembly), which is inducible by the presence of lipids, enhances the GTP hydrolysis activity of mammalian dynamins (Warnock *et al.*, 1996). In our GTP hydrolysis assay, with the addition of negatively charged lipids, a drastic increase of the GTPase activity of wild-type DYN-1 was detected, at the same rate and level as detected from rat dynamin (Figure 3B). Thus, the enhancement of GTPase activity by lipid-stimulated assembly is conserved in *C. elegans* DYN-1. In contrast, we found that the presence of lipid did not further enhance the intrinsic GTPase activity of DYN-1(I401F) (Figure 3C). This lack of enhancement strongly suggests that the DYN-1(I401F) protein is deficient in self-assembly and/or lipid attachment.

I401F Disrupts the Self-Assembly of DYN-1 *In Vitro*

We directly examined the effect of DYN-1 mutations toward the self-assembly of DYN-1 over lipids by using negative-stain TEM (data not shown) as well as cryogenic-TEM (Figure 4; see *Materials and Methods*). As reported previously for human dynamin (Sweitzer and Hinshaw, 1998; Danino *et al.*, 2004), we observed that wild-type DYN-1 assembled onto lipid surfaces and transformed liposomes into long, 50-nm-diameter tubules decorated with a helical assembly of DYN-1 (Figure 4A). DYN-1(G40E) and DYN-1(K46A) behaved exactly like wild-type DYN-1 when incubated with liposomes (Figure 4B; data not shown). This result indicates that DYN-1's self-assembly activity is independent of its GTP binding or hydrolysis. In contrast, DYN-1(I401F) failed to assemble along lipid surface or to transform liposomes into tubules (Figure 4C), demonstrating that the I401F mutation specifically disrupts DYN-1's self-assembly activity and its stable association with lipids.

The GTPase Domain Mutations Disrupt the Dissociation of DYN-1 from Lipids

Previous reports showed that in cryo-electron microscopy (EM) assays similar to the assays performed here, decorated human dynamin-lipid tubes undergo conformational changes upon GTP hydrolysis, resulting in the constriction of the underlying membrane (Danino *et al.*, 2004). We observed, within 7 s of the addition of GTP to lipid tubes decorated with wild-type DYN-1, an immediate constriction of lipid tubes in the radial dimension and of the helical pattern in the axial dimension, as was reported for human dynamin (Danino *et al.*, 2004), and the subsequent disassembly of DYN-1, as was also observed with human dynamin (Danino, unpublished data). In consequence, bare liposomes without DYN-1 decoration became abundant (Figure 4D, black arrowheads). Twisted and constricted DYN-1-lipid complexes, which are intermediates of this dissociation process, also appeared (Figure 4D, white arrowheads). Over time, undecorated vesicles became the major population detected under cryo-EM (data not shown). In contrast, no morphological changes took place in DYN-1(G40E)- or DYN-1(K46A)-coated lipid tubes upon GTP treatment (Figure 4E; data not shown). These mutant DYN-1 proteins remained assembled on lipids as helices, maintaining the diameter of lipid tubules of 50 nm. These results support the notion that GTP hydrolysis of DYN-1 leads to the constriction of lipid tubes and dissociation of dynamin from lipid surfaces (Danino, unpublished data) (Danino *et al.*, 2004).

DYN-1 Oligomerizes in *C. elegans* Cells in a Middle Domain-dependent Manner

The above-mentioned results suggest that DYN-1 undergoes self-assembly in the presence of lipids and that DYN-1 self-assembly is necessary for its enhanced GTP hydrolysis activity. Consistently, we detected a strong interaction between wild-type full-length DYN-1 in a yeast two-hybrid assay (Supplemental Figure S2). To directly visualize the interaction between DYN-1 monomers in living *C. elegans*, we established a BiFC assay. In this assay, GFP or its variant is split into two nonfluorescent moieties, each of which fused to a protein of interest, and the fusion proteins are coexpressed simultaneously. If the binding of the two po-

tential interacting partners should bring two parts of GFP to a sufficiently close distance, a functional fluorophore would form, resulting in the production of fluorescence signal (Figure 5A; (Hu *et al.*, 2002; Shyu *et al.*, 2008). DYN-1, DYN-1(I401F), and DYN-1(Δ MD) (middle domain deletion) were tagged separately with the N-terminal (residues 1-173, VN173) or C-terminal fragments (residues 155-238, VC155) of Venus, a modified form of GFP (Nagai *et al.*, 2002; Hiatt *et al.*, 2008; Shyu *et al.*, 2008). The BiFC complex formation is essentially irreversible: once formed, a GFP complex remains intact even if the interacting proteins dissociate from each other (Hu *et al.*, 2002). To avoid the potentially detrimental cellular and developmental effects of an irreversible BiFC complex, the fusion cDNAs were engineered under the control of heat-shock promoter $P_{hsp-16/41}$, which is silent at the permissive temperature for worm growing (20°C) but inducible by heat-shock (33°C), with the highest-level expression detected in intestinal cells in embryos (Stringham *et al.*, 1992; Shyu *et al.*, 2008). After heat-shock treatment (see *Materials and Methods*), we observed two distinct types of fluorescence signals in embryos and larvae expressing both DYN-1::VN173 and DYN-1::VC155 (Figure 5, B and D): I) bright, continuous fluorescent signal along the apical surface of intestinal cells (Figure 5, Ba and Da, arrowheads), and II) fluorescent puncta localized to the surface of embryos and larvae (Figure 5 Ba and Da, arrows). We interpret type II signal as nonspecific noise signal due to the fact that it was also observed in negative control embryos expressing bFos::VN173 and DYN-1::VC155 (Figure 5Be). Similar nonspecific signal was also seen in embryos expressing DYN-1(I401F) or DYN-1(Δ MD) BiFC constructs (Figure 5B, b–d). Such nonspecific signal may be derived from nonspecific aggregation of BiFC fusion proteins, similar to that reported by Kerppola (2006) and Shyu *et al.* (2008).

In contrast, type I signal is specifically from the interaction between DYN-1 molecules. In embryos expressing wild-type DYN-1 BiFC constructs, this signal was observed throughout the entire intestinal track, extending from the posterior of the second pharyngeal bulb to the anus (Figure 5B, a and g). Yet, it was absent from the negative-control embryos (Figure 5Be). This specific BiFC signal representing the interaction of DYN-1 monomers along the apical surface of intestinal cells is consistent with the essential role of DYN-1 for endocytosis (Grant and Hirsh, 1999). In contrast, the heat-shock-induced expression of DYN-1(I401F)::VN173 and DYN-1(I401F)::VC155, although produced fusion proteins of predicted sizes and of levels equivalent to that of wild-type fusion proteins (Supplemental Figure S3), resulted in primarily no or only partial fluorescent lines along the intestinal track in wild-type embryos or larvae (Figure 5B, b and h; C; and D, c and d). The same mutant DYN-1 BiFC constructs, when expressed in *dyn-1(en9)* mutant embryos where no endogenous functional DYN-1 was available, created an even more prominent defect in BiFC signals—the fluorescent line along the intestinal track was absent from all embryos (Figure 5B, c and i, and C). These results indicate that the I401F mutation severely impairs DYN-1's self-assembly in vivo. Like that of DYN-1(I401F), the DYN-1(Δ MD) fusion proteins (Supplemental Figure S3) did not generate any specific BiFC signal on the apical surface of intestinal track (Figure 5B, d and j), further indicating that the middle domain is needed for DYN-1's in vivo self-interaction.

Based on the BiFC assay results, and on the observation that the GTPase domain mutations of DYN-1 induces dominant-negative effects in the removal of cell corpses (see the next section), we further developed a genetic assay that

demonstrated the essential function of DYN-1 oligomerization in vivo (see the next section).

Self-Assembly-deficient Mutations Suppress the Dominant-Negative Effects of the GTPase Domain Mutations In Cis

We found that the transgenic expression of *dyn-1* cDNA bearing individual mutations G40E, K46A, and G204E defective in GTP binding as a *gfp* fusion, under the control of a pair of heat-shock promoters $P_{hsp-16/2}$ and $P_{hsp-16/41}$ (collectively referred to as P_{hsp}), caused dominant-negative Ced and Emb phenotypes in an otherwise wild-type background (Figure 6; data not shown). After heat-shock treatment (see *Materials and Methods*), ~20 cell corpses in late fourfold stage embryos accumulate in embryos carrying these transgenes, when there are nearly no detectable cell corpses in wild-type embryos carrying no transgene (Figure 6). In two transgenic lines expressing DYN-1(G204E), 40 and 80% transgenic animals die in embryonic stage after heat-shock. Both the Ced and Emb phenotypes are similar to that observed from homozygous *dyn-1* loss-of-function mutants (Yu *et al.*, 2006), indicating that these mutations not only inactivate the transgenic DYN-1::GFP molecules in cis but also severely interfere with the function of endogenous wild-type DYN-1 in trans.

In contrast, the heat-shock induced expression of DYN-1(I401F) in wild-type embryos, although leading to the production of an amount of GFP fusion protein similar to DYN-1(G40E) (Figure 6A, e and f, and C), does not result in the accumulation of cell corpses (Figure 6) or embryonic lethality (data not shown). In addition, R402A, another middle domain mutation in DYN-1, which corresponds to R399A in human dynamin 1, a mutation that was reported to disrupt dynamin tetrameric structure in vitro (Ramachandran *et al.*, 2007), failed to cause dominant Ced or Emb phenotypes, although the mutant protein was induced to express by heat-shock at a relatively equivalent level (Figure 6, B and C). These results indicate that although these two middle domain mutant DYN-1 molecules are inactive (Figure 2 and Supplemental Figure S1), unlike GTPase domain mutant DYN-1, they do not interfere with the function of endogenous wild-type DYN-1.

If the dominant-negative effect of DYN-1 molecules carrying mutations in the GTPase domain is caused by their interference of the endogenous wild-type DYN-1 molecules in the same polymer, a second mutation that inactivates the oligomerization activity of the very mutant molecules should suppress their dominant-negative effect. We tested this hypothesis by introducing GTPase and middle domain double mutations into the *dyn-1* heat-shock induction constructs. We found that the heat-shock induced expression of *dyn-1*(G40E I401F) double mutant cDNA failed to induce any dominant-negative phenotype in cell corpse removal (Figure 6) or embryonic development (data not shown). DYN-1(G40E I401F)::GFP displayed a bright fluorescence signal (Figure 6Ag) and a protein level similar to that of DYN-1(G40E)::GFP or DYN-1(I401F)::GFP (Figure 6C), indicating that the lack of dominant-negative effect is not due to lack of protein production or reduced protein stability. Similarly, I401F also suppresses the dominant-negative effect of G204E in cis (Figure 6, B and C, and Supplemental Figure S4). In addition, the mutation R402A also suppresses the dominant-negative effect of G40E in cis without significantly affecting the protein level, suggesting the suppression effect is common to middle domain mutations (Figure 6, B and C; and Supplemental Figure S4). That the dominant-negative effect of GTPase domain mutant DYN-1 relies on the self-

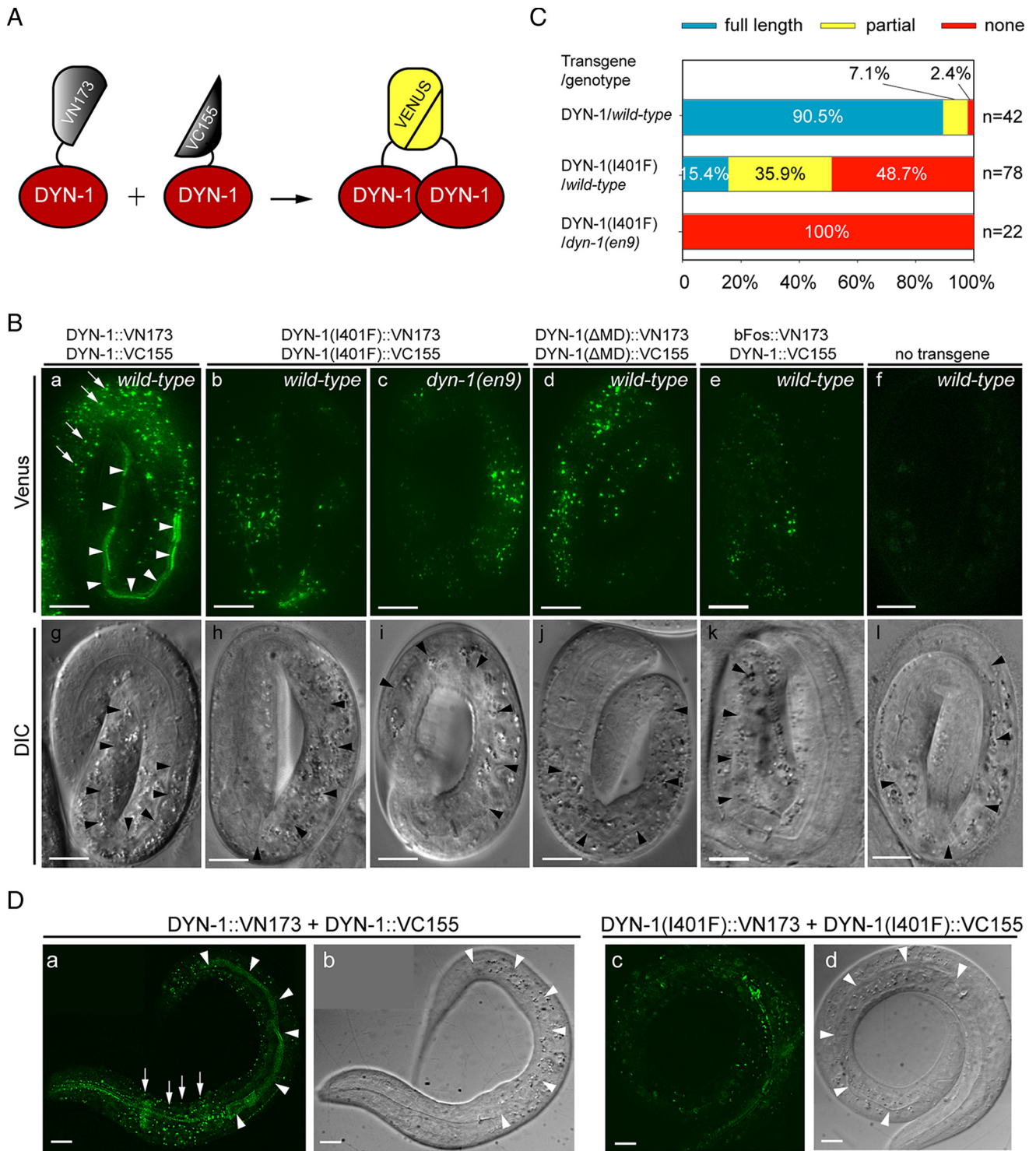


Figure 5. The I401F mutation impairs DYN-1 oligomerization in *C. elegans*. (A) Diagram illustrating the principle of the BiFC assay. DYN-1 is fused with each one of the two fragments of Venus, VN173 (Venus 1-173 aa) or VC155 (Venus 155-238 aa) and expressed in the target cells. The appearance of a yellow fluorescence signal indicates the detectable interaction between DYN-1 monomers. (B) Fluorescence (a–f) and corresponding DIC (g–l) images of fourfold stage wild-type or *dyn-1(en9)* homozygous embryos expressing different BiFC constructs. Each fluorescence image represents two-dimensional projection of five consecutive 1- μ m z-sections. Arrowheads indicate the fluorescence signals detected along the apical surface of the intestinal cells. Arrows indicate the fluorescent puncta observed throughout the worm body and considered nonspecific aggregation products. Bars, 10 μ m. (C) Quantification of BiFC-positive intestinal tracks scored from embryos expressing different BiFC constructs. The percentage of embryos with fluorescent signal labeling the full-length (from the end of the second pharyngeal bulb to anus) or part of the intestinal track or with no signal along the entire intestinal track are represented in blue, yellow, or red, respectively. n, number of embryos scored. (D) Fluorescence (a and c) and corresponding DIC (b and d) images of L1 wild-type larvae expressing BiFC constructs. Arrowheads indicate the fluorescence signals detected along the apical surface of the intestinal cells. Arrows indicate the fluorescent puncta considered nonspecific aggregation products. Bars, 10 μ m.

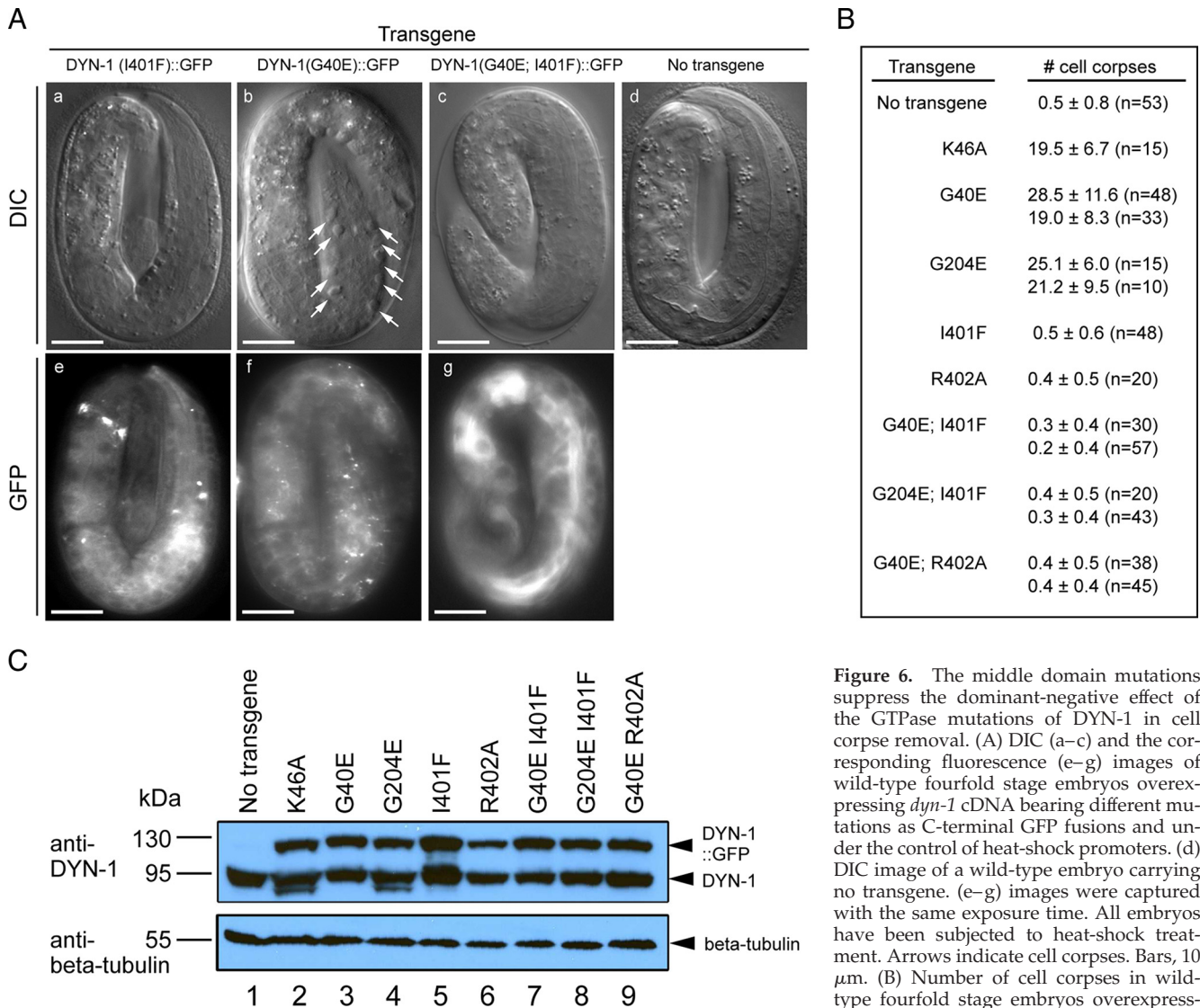


Figure 6. The middle domain mutations suppress the dominant-negative effect of the GTPase mutations of DYN-1 in cell corpse removal. (A) DIC (a–c) and the corresponding fluorescence (e–g) images of wild-type fourfold stage embryos overexpressing *dyn-1* cDNA bearing different mutations as C-terminal GFP fusions and under the control of heat-shock promoters. (d) DIC image of a wild-type embryo carrying no transgene. (e–g) images were captured with the same exposure time. All embryos have been subjected to heat-shock treatment. Arrows indicate cell corpses. Bars, 10 μ m. (B) Number of cell corpses in wild-type fourfold stage embryos overexpressing *dyn-1* cDNA bearing different mutations as C-terminal GFP fusions and under the control of heat-shock promoters. For each transgene (except K46A, I401F, and R402A), the results from two independent transgenic lines are presented. Data are presented as mean \pm SD, and n is number of embryos scored. (C) Western blots of *C. elegans* protein extracts probed with polyclonal antibodies against DYN-1 (top) and β -tubulin (bottom). The predicted sizes of endogenous DYN-1 and DYN-1::GFP are 93 and 130 kDa, respectively. All samples have been treated with heat-shock and harvested 3 h later.

as C-terminal GFP fusions and under the control of heat-shock promoters. For each transgene (except K46A, I401F, and R402A), the results from two independent transgenic lines are presented. Data are presented as mean \pm SD, and n is number of embryos scored. (C) Western blots of *C. elegans* protein extracts probed with polyclonal antibodies against DYN-1 (top) and β -tubulin (bottom). The predicted sizes of endogenous DYN-1 and DYN-1::GFP are 93 and 130 kDa, respectively. All samples have been treated with heat-shock and harvested 3 h later.

assembly activity of DYN-1 strongly indicates that the in vivo self-assembly activity of DYN-1 is essential for its functions in the removal of cell corpses and embryonic development.

DYN-1 Self-Assembly Is Essential for the Association between DYN-1 and Its Target Membranes in C. elegans Cells

To study whether self-assembly of DYN-1 plays a role in DYN-1's subcellular localization, we examined the effect of DYN-1 mutations toward the localization of DYN-1::GFP. The transgenes were placed under the control of the engulfing cell-specific *ced-1* promoter (Zhou *et al.*, 2001b; Yu *et al.*, 2006) and expressed in wild-type or the corresponding homozygous mutant embryos. We characterized DYN-1 localization in cells in which DYN-1 is essential for cellular function, including intestinal cells, where it plays an essen-

tial role in endocytosis, and hypodermal cells, where it actively promotes the engulfment and degradation of apoptotic cells (Grant and Hirsh, 1999; Yu *et al.*, 2006).

In intestinal cells, DYN-1::GFP is enriched along the apical surface toward the intestinal lumen (Figure 7A), consistent with the active self-assembly of DYN-1 in this region detected by the BiFC assay (Figure 5). In contrast, DYN-1(I401F)::GFP seems to reside in the cytoplasm in a diffused pattern in wild-type embryos, and also in *dyn-1(en9)* mutant embryos, where there is no wild-type DYN-1 molecules to stimulate assembly (Figure 7B). No significant enrichment on any cellular structures, either the apical surface of intestinal cells or the surfaces of pseudopods or phagosomes, was observed in 1.5-fold embryos (Figure 7B) or embryos at other developmental stages (data not shown).

To determine the localization of DYN-1(I401F) during the engulfment and degradation of apoptotic cells, we moni-

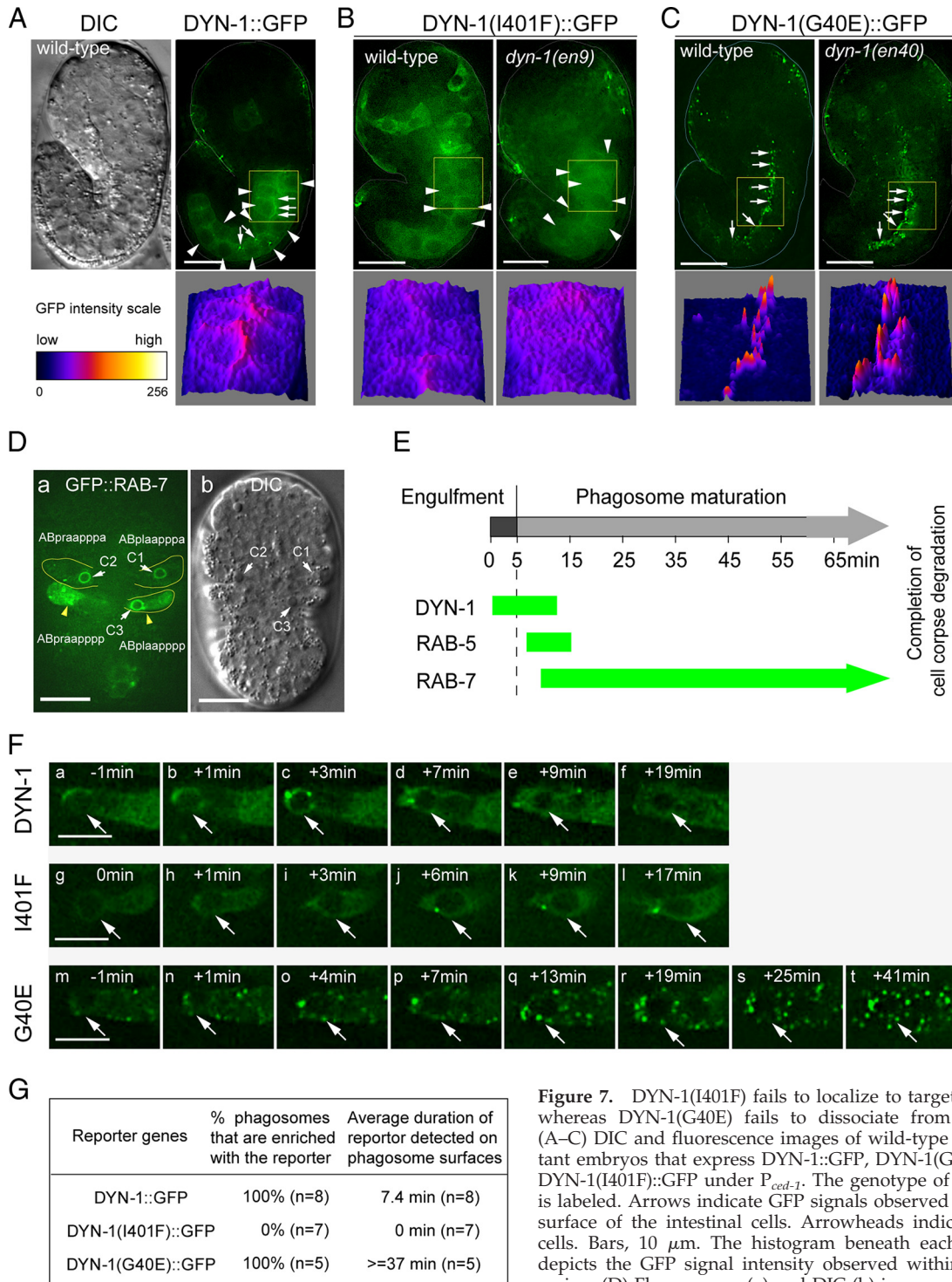


Figure 7. DYN-1(I401F) fails to localize to target membranes, whereas DYN-1(G40E) fails to dissociate from membranes. (A–C) DIC and fluorescence images of wild-type or *dyn-1* mutant embryos that express DYN-1::GFP, DYN-1(I401F)::GFP, or DYN-1(G40E)::GFP under P_{ced-1} . The genotype of each embryo is labeled. Arrows indicate GFP signals observed on the apical surface of the intestinal cells. Arrowheads indicate intestinal cells. Bars, 10 μ m. The histogram beneath each GFP image depicts the GFP signal intensity observed within the framed region. (D) Fluorescence (a) and DIC (b) images of a wild-type embryo expressing $P_{ced-1} gfp::rab-7$ at \sim 330 min postfirst-embryonic

division. Phagosomes C1, C2, and C3 are labeled with enriched GFP::RAB-7 (arrows). The boundary of three ventral hypodermal cells (identities labeled) that have engulfed apoptotic cells C1, C2, and C3 are traced with yellow lines. Yellow arrowheads indicate two hypodermal cells that fuse at the ventral midline of the embryo. This fusion event is used as a landmark of embryonic development with which the timing of engulfment is compared with in Figure 10. Anterior is to the top. Ventral faces readers. Bars, 10 μ m. (E) Temporal order and duration of the enrichment of DYN-1, RAB-5, and RAB-7 on phagosomal surfaces. Data represent mean values obtained from time-lapse recording monitoring through the engulfment and degradation processes of multiple C1, C2, and C3 cell corpses using GFP fused reporters in wild type embryos. 0 min represents the time point when budding pseudopods are first detected. (F) Time-lapse images of wild-type embryos that express DYN-1::GFP (a–f), DYN-1(I401F)::GFP (g–l), or DYN-1(G40E) (m–t) under P_{ced-1} . Arrows indicate C3 phagosomes. 0 min is the time point when engulfment is just completed. Bars, 5 μ m. (G) The frequencies of phagosomes C1, C2, and C3 labeled with enriched DYN-1::GFP reporters in a period >30 min, starting when engulfment is complete, and the average duration of GFP on phagosomal surfaces. In this series of time-lapse experiments, our recording terminated at \sim 40 min after the completion of engulfment. n, number of C1, C2, and C3 phagosomes recorded.

tored each of these processes of three particular apoptotic somatic cells, C1, C2, and C3, by using a time-lapse recording technique established previously (Yu *et al.*, 2006). C1, C2, and C3, which are located close to the ventral surface of an embryo, undergo apoptosis at approximately the same time (~330 min after the first embryonic cell division), and are engulfed by their neighboring ventral hypodermal cells ABplaappppa, ABpraappppa, and ABplaappppp, respectively (Figure 7D; Yu *et al.*, 2006). Throughout the engulfment and degradation processes of cell corpses C1, C2, and C3, the clustering of DYN-1::GFP signal around these cell corpses reaches its peak shortly after engulfment completes (Figure 7, E and F), as reported previously (Yu *et al.*, 2006, 2008). Within 10 min, the transient clustering disappears and a phagosome is detected as a dark hole in the engulfing cell cytosol (Figure 7, E and Fd). In embryos that express DYN-1(I401F)::GFP, however, GFP does not enrich around phagocytic cup or nascent phagosomes at any moment throughout the engulfment and degradation process (Figure 7F, g-l; data not shown), indicating that the assembly-defective I401F mutation abolishes DYN-1's ability to associate with phagocytic membranes. The above-mentioned results thus indicate that self-assembly of DYN-1 is essential for the *in vivo* association of DYN-1 with target membranes.

The GTP Binding Mutation Results in a Severe Defect in DYN-1's Dissociation from Target Membranes *In Vivo*

In both wild-type and *dyn-1(en40)* mutant embryos that expressed DYN-1(G40E)::GFP, high level GFP signal was observed on the apical surface of intestinal cells (Figure 7C), indicating that the GTP binding activity is not essential for DYN-1 association with target membranes. Interestingly, the level of enrichment of DYN-1(G40E)::GFP signal on apical surfaces of intestinal cells is higher than that of DYN-1::GFP (Figure 7, A and C), suggesting that either DYN-1(G40E) displays a higher affinity to target membrane than DYN-1 or that it does not dissociate from the target membranes efficiently. Our time-lapse recording throughout the removal processes of C1, C2, and C3 further indicates two abnormal aspects of DYN-1(G40E) localization to phagosomal surfaces. First, the peak of DYN-1(G40E)::GFP signal detected on the surface of nascent phagosomes is higher and reached later than that of DYN-1::GFP in relation to the engulfment process (Figure 7F, m-p). Second, more strikingly, after reaching the intensity plateaus, the DYN-1(G40E)::GFP signal persists on phagosomal surfaces for a much longer time period compared with DYN-1::GFP (Figure 7E; F, q-t; and G). These observations strongly indicate that there is a profound defect in DYN-1(G40E)'s dissociation from phagosomal membranes, as observed in cryo-EM experiments *in vitro* (Figure 4), and they further suggest that, among other defects resulted from this mutation, a defect in membrane dissociation is likely to contribute to the failure of DYN-1(G40E) to promote the removal of apoptotic cells.

In addition, in hypodermal cells, DYN-1(G40E)::GFP accumulates at a high concentration on cytoplasmic puncta, which might represent intracellular organelles (Figure 7F, m-t; Yu *et al.*, 2006). The degree of aggregation of DYN-1(G40E) cytoplasmic puncta is higher than that of wild-type DYN-1 (Yu *et al.*, 2006), indicating that the G40E mutation might also affect the dynamic dissociation of DYN-1 from intracellular organelles.

Both the GTPase and the Self-Assembly Mutations Cause Severe Defect in the Degradation of Apoptotic Cells

The *dyn-1(en9)* and *dyn-1(en40)* homozygous embryos from heterozygous mothers carry a large number of persistent cell

corpses, indicating a severe cell corpse removal defect (Figure 8B, m^+z^- embryos) (*m*, maternal gene product; *z*, zygotic gene product). When the wild-type maternal *dyn-1* product was further depleted from the homozygous mutant embryos (see *Materials and Methods*), the cell corpse removal defect was further enhanced (Figure 8, A and B m^-z^- embryos). We monitored the degradation process of C1, C2, and C3 and found that, like *dyn-1(n4039)(G204E)* mutant embryos (Yu *et al.*, 2006, 2008), the *en9* and *en40* embryos are severely defective in the degradation of apoptotic cells.

We measured the duration of phagosomes using the CED-1C::GFP reporter, a fusion protein between the cytoplasmic domain of CED-1 and GFP. CED-1C::GFP, which is expressed under the control of the *ced-1* promoter, is evenly distributed in the cytoplasm of engulfing cells and allows the recognition of phagosomes as GFP(-) holes in a GFP(+) background (Figure 8B; Yu *et al.*, 2008). In wild-type embryos, the degradation of phagosomal content leads to the gradual reduction of phagosome size. One-hundred percent of C1, C2, and C3 phagosomes are totally degraded within 60 min after the engulfment is completed, among which 89% are degraded within 50 min (Figure 8, C and D). On the contrary, only 21.1 and 31.8% of phagosomes in *dyn-1(en9)* and *dyn-1(en40)* embryos, respectively, were fully degraded within 60 min. In addition, 15.8 and 22.7% of phagosomes in *dyn-1(en9)* and *dyn-1(en40)* embryos, respectively, lasted >80 min (Figure 8, C and D). These results indicate that the loss of the GTP binding or self-assembly activities severely affect DYN-1's functions in the degradation of cell corpses.

The Defects in Phagosome Maturation Caused by the I401F Mutation Are Closely Associated with the Defect in RAB-7 Recruitment

Previously, we found that the phagosome maturation defects caused by DYN-1 mutations were directly related to the severe defects in the delivery and fusion of early endosomes and lysosomes to phagosomes, vesicle trafficking events that are essential for providing digestive enzymes to and the acidification of phagosome lumen (Yu *et al.*, 2006, 2008). To determine the contribution of DYN-1's self-assembly and GTP binding activities to these vesicle/phagosome fusion events, we analyzed the effects of two classes of DYN-1 mutations on the recruitment of two distinct membrane tethering factors, the small GTPases RAB-5 and RAB-7 (Cai *et al.*, 2007), to phagosomal surfaces. We found previously that the function of RAB-7 on phagosomal surfaces was essential for the recruitment and fusion of lysosomes but not early endosomes to phagosomal membranes (Yu *et al.*, 2008). Using an engulfing cell-specific GFP::RAB-7 reporter developed previously (Yu *et al.*, 2008), we monitored the dynamic recruitment of RAB-7 to phagosomal surfaces. In wild-type worms, >90% of phagosomes were labeled with high concentrations of GFP::RAB-7 within 10 min after engulfment is completed and until their complete degradation (Figures 7E, 9, Aa and B; and Supplemental Movie S1; Yu *et al.*, 2008). After RAB-7 recruitment, phagosomes started to reduce in size until complete disappearance within 60 min (Figure 9, Aa and B, and Supplemental Movie S1). In contrast, in *dyn-1(en9)* mutant embryos, 33.3% of phagosomes remained RAB-7(-) for the entire recording period of 100 min, all of which remained undegraded throughout the recording period (Figure 9, Ab and C, a-e; and Supplemental Movie S2). In addition, on the surface of 22.2% of phagosomes, GFP::RAB-7 was briefly enriched yet quickly disappeared, indicating a defect in maintaining RAB-7 on phagosomal surfaces; likewise, these phagosomes failed to reduce in size throughout the recording time of 100 min (Figure 9A, c and

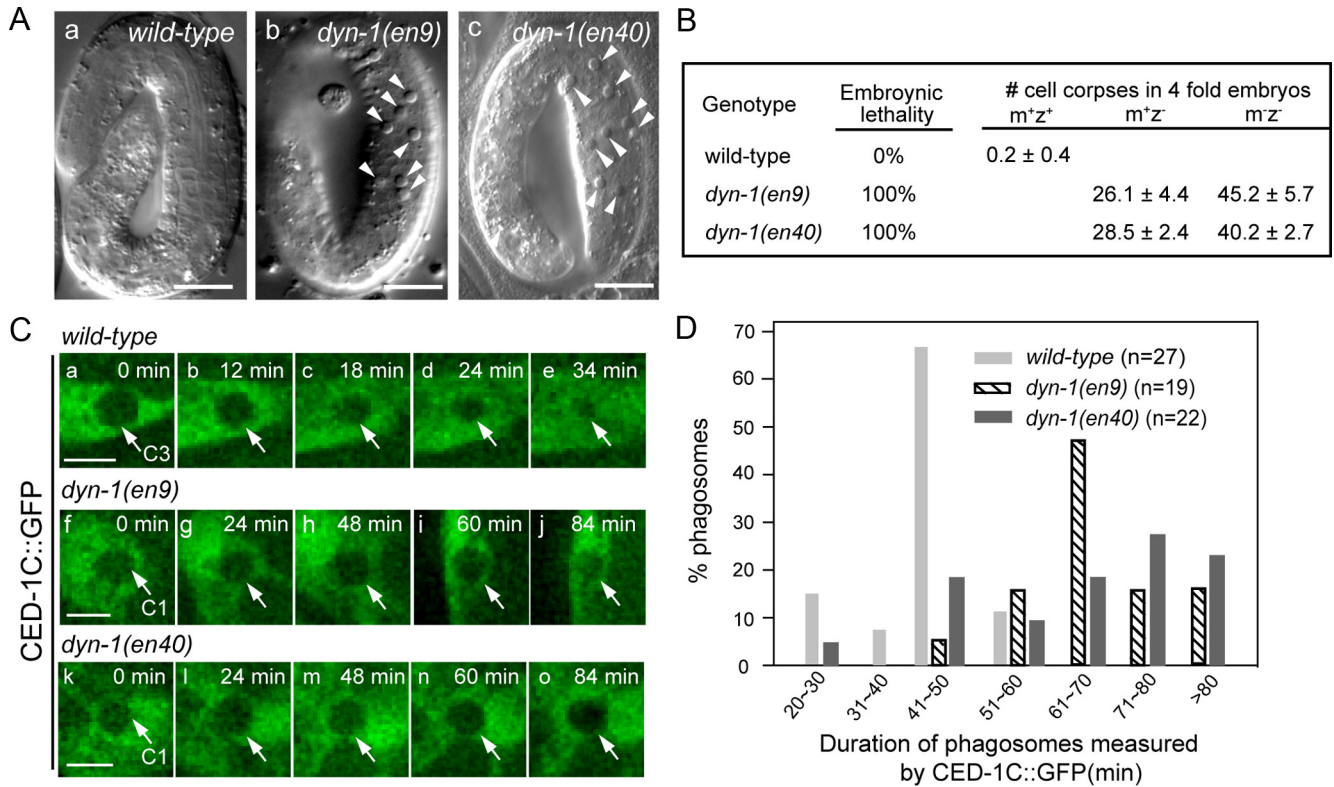


Figure 8. Both the G40E and I401F mutations severely impair the degradation of apoptotic cells. (A) *dyn-1(en9)* and *dyn-1(en40)* homozygous embryos carry persistent cell corpses. (a–c) DIC images of fourfold stage wild-type embryos and homozygous *dyn-1(en9)* (m^+z^-) and *dyn-1(en40)* (m^-z^-) embryos generated by homozygous mother rescued by wild-type *dyn-1* genomic fragment as extrachromosomal array. Arrowheads indicate cell corpses. Scale bars: 10 μ m. (B) The number of cell corpses (mean \pm sd) and percentage embryonic lethality observed from homozygous (m^+z^+) mutant embryos generated by heterozygous mothers and from (m^-z^-) mutant embryos generated by homozygous mother rescued by wild-type *dyn-1* genomic fragment as extrachromosomal array. (C) Time-lapse images of embryos expressing $P_{ced-1}ced-1::gfp$ that demonstrate the duration of phagosomes in different genetic backgrounds. 0 min: the time point when engulfment is just complete and a phagosome (arrows) is first detectable as a dark hole inside the engulfing cell. Scale bars are 2 μ m. (a–e) images of a C3 phagosome in a wild-type embryo. (f–j) images of C1 phagosome in *dyn-1(en9)* embryos. (k–o) images of C1 phagosome in *dyn-1(en40)* embryos. (D) Histogram distribution of phagosomal durations in embryos determined using CED-1C::GFP as a reporter. Duration is measured from the formation of a nascent phagosome until its degradation. n, number of phagosomes C1, C2 and C3 measured using time-lapse recording.

d; and C, f–k). In the rest of phagosomes (44.4%), the recruitment of RAB-7 to phagosomal surfaces was delayed to various extents (Figure 9A, e and f; and C, l–q), and the degradation of the corresponding phagosomes was delayed to equivalent levels. These observations strongly indicate that DYN-1 self-assembly and targeting to phagosomal membrane are critical for the recruitment of the RAB-7 GTPase.

The GTP Binding Mutation G40E Does Not Severely Affect the Enrichment of RAB-7 to Phagosomal Surfaces

In contrast to the severe RAB-7 recruitment defects observed in *dyn-1(en9)* mutants, in *dyn-1(en40)* mutant embryos, the defects in the dynamic recruitment of GFP::RAB-7 to phagosomal surfaces were relatively weak and only influence a small percentage of phagosomes (Figure 9A, g–k; and D). On the surfaces of 80% of phagosomes, RAB-7 was enriched within 10 min after phagosome formation (Figure 9A, g–i; and D, a–k). In the rest of phagosomes, RAB-7 was enriched between 10 and 20 min after phagosome formation (Figure 9A, j and k; and D, l–q). These observations indicate that the DYN-1(G40E) mutant protein, although deficient in GTP binding, is still able to promote the timely association of RAB-7 to phagosomal surfaces.

The relatively normal kinetics of RAB-7 recruitment seems to correlate with the relatively short delay of phagosome maturation observed when transgenic GFP::RAB-7 is expressed in *dyn-1(en40)* mutant embryos. In particular, among the 12 phagosomes onto which RAB-7 was recruited within 10 min of phagosome formation, the duration of eight phagosomes was shorter than 70 min (Figure 9A, g–h). In addition, the duration of the three phagosomes on which RAB-7 was recruited between 10 and 20 min after phagosome formation ranges between 64 and 86 min (Figure 9A, j and k), merely 16–56% longer than the 55-min average phagosome duration observed in wild-type cells (Figure 9Aa). Comparing to the drastically prolonged phagosome duration observed in *dyn-1(en9)* mutants that also expressed GFP::RAB-7 (Figure 9A, b–f), the expression of GFP::RAB-7 seemed to partially suppress the prolonged phagosome maturation phenotype in *dyn-1(en40)* mutants (Figure 9A, g–k).

However, the suppression activity of GFP::RAB-7 transgene does not seem to be fully penetrant. In particular, four of the 12 phagosomes onto which RAB-7 was recruited within the normal time frame (10 min) existed for a period between 81 and 108 min (Figure 9Ai and D, f–k). This phenomenon suggests that there are other essential events for phagosome maturation that could be affected by the

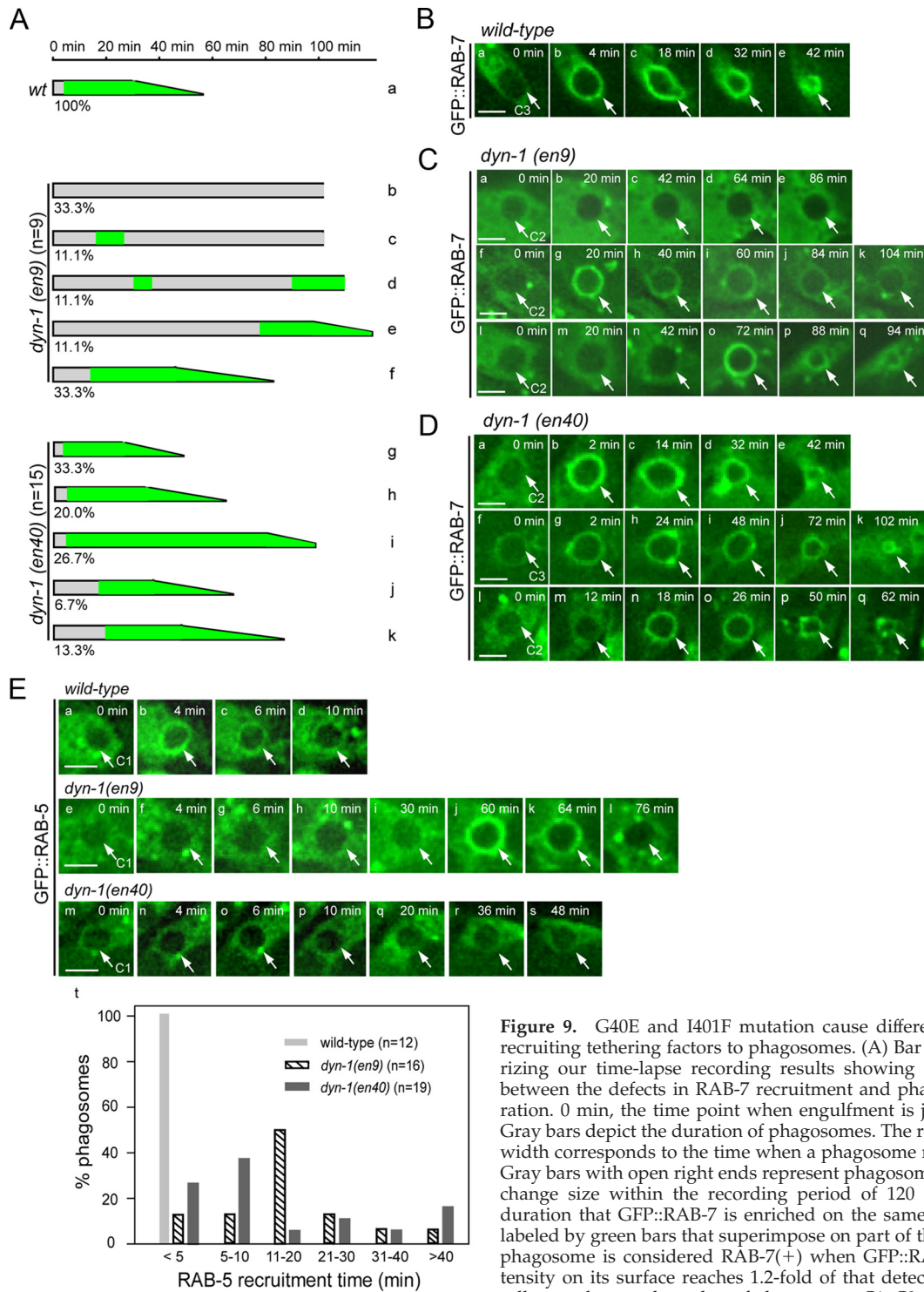


Figure 9. G40E and I401F mutation cause differential effects in recruiting tethering factors to phagosomes. (A) Bar graph summarizing our time-lapse recording results showing the correlation between the defects in RAB-7 recruitment and phagosome maturation. 0 min, the time point when engulfment is just completed. Gray bars depict the duration of phagosomes. The reduction of bar width corresponds to the time when a phagosome reduces in size. Gray bars with open right ends represent phagosomes that did not change size within the recording period of 120 min. The time duration that GFP::RAB-7 is enriched on the same phagosome is labeled by green bars that superimpose on part of the gray bars. A phagosome is considered RAB-7(+) when GFP::RAB-7 signal intensity on its surface reaches 1.2-fold of that detected in the host cell cytosol. n, total number of phagosomes C1, C2, and C3 scored.

(B–D) Time-lapse images of one C3 (B) and multiple C2 (C–D) phagosomes in embryos expressing $P_{ced-18}::gfp::rab-7$. 0 min, the time point when engulfment is just completed and the C2 phagosome (arrows) is first detectable as a dark hole inside its engulfing cell. Bars, 2 μ m. (B) Images of a C3 phagosome in a wild-type embryo. (C) Time-lapse images of three different phagosomes (a–e, f–k, and l–q) in *dyn-1(en9)* embryos. (D) Time-lapse images of three different phagosomes (a–e, f–k, and l–q) in *dyn-1(en40)* embryos. (E) Time-lapse images of embryos expressing $P_{ced-18}::gfp::rab-5$ for measuring the recruitment of RAB-5 to phagosomal surfaces. 0 min, the time point when engulfment is just completed and the C1 phagosome (arrows) is first detectable as a dark hole inside the engulfing cell. Bars, 2 μ m. (a–s) Images of C1 phagosomes in wild-type (a–d), *dyn-1(en9)* (e–l), and *dyn-1(en40)* (m–s) embryos. (t) Histogram indicating the distribution of the time point when RAB-5 is first recruited to phagosomal surfaces measured using GFP::RAB-5 as a reporter, which is defined as the first time point when the GFP signal intensity on phagosomal surfaces is at least 1.2-fold as high as that in the cytosol of the cell that hosts the phagosome. 0 min is the time point when engulfment is just completed. n, number of phagosomes C1, C2, and C3 measured using time-lapse recording.

G40E mutation in endogenous *dyn-1*. We further examined the dynamic phagosomal localization of RAB-5, a tethering factor between early endosomes and phagosomes, in the *dyn-1(en9)* and *dyn-1(en40)* mutant embryos.

Both *dyn-1(en9)* and *dyn-1(en40)* Mutants Are Defective in the Recruitment of RAB-5 to Phagosomes

The small GTPase Rab5 is enriched on maturing phagosomes (Vieira *et al.*, 2002; Kinchen *et al.*, 2008; Kitano *et al.*, 2008). Using a GFP::RAB-5 reporter expressed in engulfing cells under the control of the *ced-1* promoter that we constructed, we monitored the dynamic recruitment and duration of *C. elegans* RAB-5 on phagosomes C1, C2, and C3. In wild-type embryos, we observed that GFP::RAB-5, which was evenly distributed in the cytoplasm, was recruited to phagosomal surfaces within 4 min after the completion of engulfment and remained there for an average of 9 min (Figures 7E and 9E, a–d and t; and Supplemental Movie S3). In both *dyn-1(en9)* and *dyn-1(en40)* homozygous embryos, however, the time points when GFP::RAB-5 was first enriched on phagosomal surfaces varied in a large range from <5 min to >40 min (Figure 9Et). Only 12.5 and 26.3% of phagosomes in *dyn-1(en9)* and *dyn-1(en40)* mutant embryos, respectively, recruited GFP::RAB-5 within 5 min like those in wild-type embryos (Figure 9E). Furthermore, 25.0 and 31.6% of phagosomes remained GFP::RAB-5(–) for 20 min or longer immediately after the formation of nascent phagosomes in *dyn-1(en9)* and *dyn-1(en40)* homozygous embryos, respectively (Figure 9E). Unlike the RAB-7 recruitment defect, the severity of the RAB-5 recruitment defect was similar between the *dyn-1(en9)* and *dyn-1(en40)* mutant backgrounds (Supplemental Movies S4 and S5). In both mutants, the duration of GFP::RAB-5 on phagosomes remained within 10 min, indicating that the transient nature of RAB-5 enrichment onto phagosomes is not changed (Supplemental Figure S5).

The GTP Binding and Self-Assembly Mutations Also Cause Engulfment Defects

We monitored the engulfment processes of cell corpses C1, C2, and C3 over time with the GFP::RAB-5 reporter used above. This reporter, although is not enriched on the surface of pseudopods (Figure 9E), is evenly distributed in the cytoplasm, allowing us to track the extension and closure of thin pseudopods over time (Figure 10A, a–e). To further determine the precise time point when engulfment was initiated during embryonic development, we used the time point when the two hypodermal cells ABplaapppp and ABpraapppp first made contact and started to fuse with each other at the embryonic ventral midline, a developmental event independent of cell corpse engulfment, as a reference point (Figure 10Aw; Yu *et al.*, 2008). In wild-type embryos, the engulfment of C1, C2, and C3 takes on average 5 min to complete and is usually completed at least 7 min before the contact between ABplaapppp and ABpraapppp is made (Figure 10A, a–e, and w) (Yu *et al.*, 2008). In *ced-1* mutant embryos known to be defective in both the engulfment and degradation of cell corpses, ~28% of C3 cell corpses fail to be engulfed within 30 min (Yu *et al.*, 2008). We classified the specific defects observed in the *en40* and *en9* mutants into four categories (Figure 10B). In the *dyn-1(en40)* background, among the 22 cell corpses that we monitored, four were not engulfed within the 60-min recording period, due to either the lack of pseudopod initiation or the failure of pseudopod extension and closure (Figure 10A, p–v); two were not fully engulfed until at least 6 min after ABplaapppp and ABpraapppp made contact due to either delayed pseudopod initiation

or slower-than-normal pseudopod extension, whereas the rest 16 were engulfed in normal kinetics (Figure 10B). Similar defects in the four categories were also observed when CED-1C::GFP, another cytosolic reporter was used to label pseudopods (Figure 10C). In *dyn-1(en9)* embryos, delay of pseudopod initiation and perturbation of pseudopod extension were also observed, albeit at a lower frequency (Figure 10C). Figure 10A, f–o, shows an example of a failure of engulfment initiation observed in *dyn-1(en9)* mutant background.

DISCUSSION

Two Novel Assays That Detect the Site-specific Self-Assembly of Dynamin In Vivo

Although the self-assembly of dynamin along lipid surface has been observed in vitro (see *Introduction*), the actual oligomerization in vivo under physiological conditions remains to be visualized directly (Takei *et al.*, 1995; Evergren *et al.*, 2004). Moreover, it is not known whether the monomeric or oligomeric form of dynamin is the active form for promoting membrane fusion.

Using *C. elegans* as a model system, we have developed two complementary assays that detect the oligomerization of dynamin in vivo. The BiFC assay allows us to not only directly detect the interaction between DYN-1 monomers but also determine the specific membrane region where the interaction occurs. On the other hand, the genetic suppression of the dominant-negative effect of the GTPase domain mutations by assembly-deficient mutations enables us to determine the functional importance of DYN-1 self-assembly. Whereas our biochemical assays have demonstrated that the middle domain mutation I401F resulted in a specific defect in DYN-1 self-assembly in vitro, the results of these two in vivo assays described above, together with the defects in phagosome maturation and engulfment and the 100% embryonic lethality observed from the assembly-deficient *dyn-1(en9(I401F))* mutant embryos, have established that DYN-1 does assemble as polymers in *C. elegans* cells and that this event is essential for its functions in the removal of cell corpses and in embryonic development (Figure 11).

Overexpression of mutant DYN-1 molecules defective in GTP binding and/or hydrolysis may interfere with the functions of endogenous wild-type DYN-1 through one of the following mechanisms: 1) as monomers, mutant DYN-1 molecules may sequester important positive regulators from wild-type DYN-1; or 2) mutant DYN-1 molecules may generate inactive DYN-1 polymers by assembling together with wild-type DYN-1. The absolute dependence of the observed dominant-negative effect on DYN-1's self-assembly activity indicates that the generation of "poisonous polymers" is the likely mechanism among the two. This genetic suppression assay thus is an efficient method for determining whether any particular dynamin mutation impairs dynamin's self-assembly in vivo.

The Contributions of the Self-Assembly and GTPase Activities to the Precise Temporal Regulation of DYN-1's Dynamic Localization on Target Membranes

Our in vivo study of the I401F mutation indicates that the self-assembly of DYN-1, which relies on its middle domain, is essential for DYN-1's association with the surface of pseudopods or phagosomes or other target membranes (Figure 11A). What is the molecular relationship between DYN-1's self-assembly and the association with target membranes? Despite the obvious link between the PH domain and the

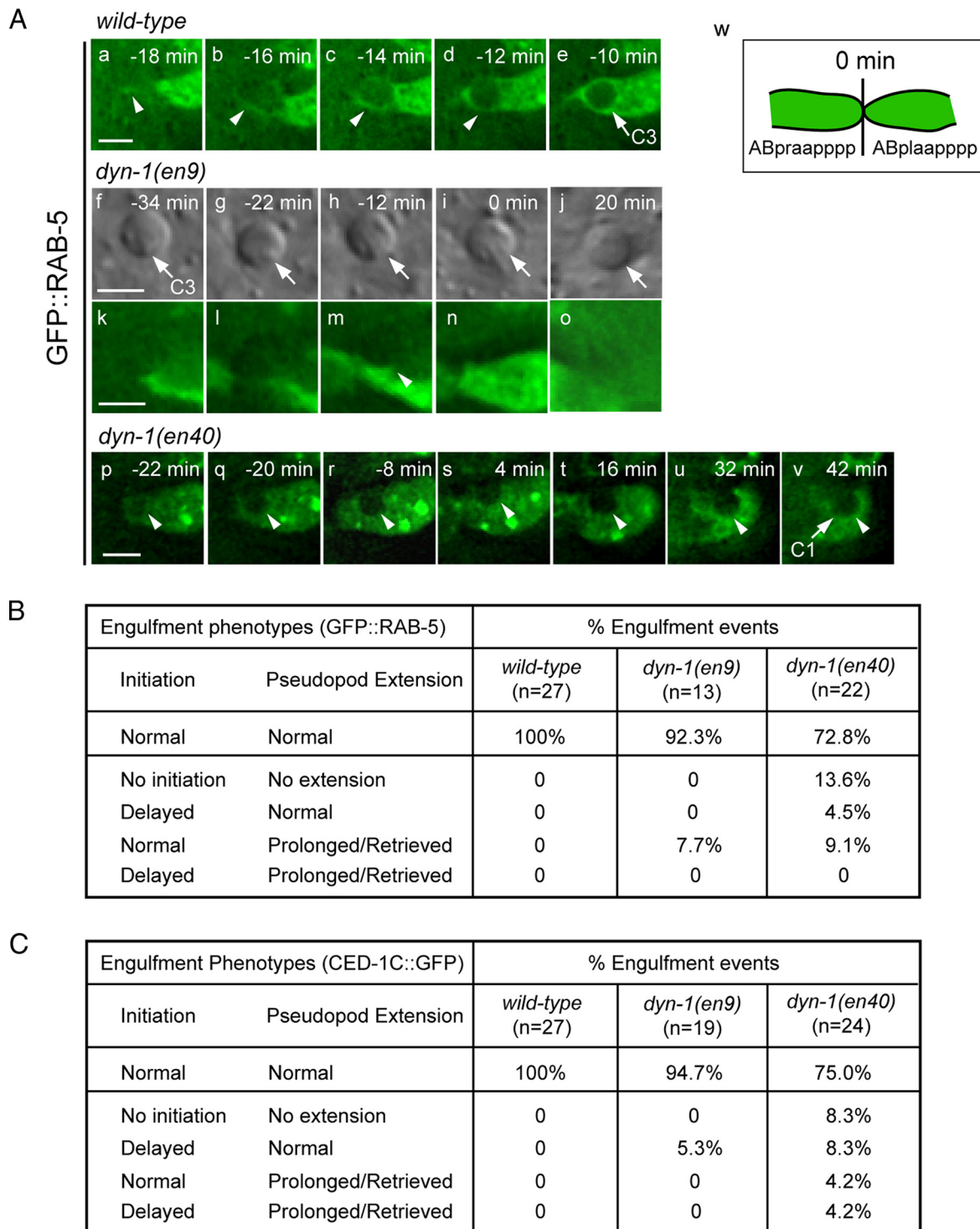


Figure 10. Both G40E and I401F mutations impair the engulfment of apoptotic cells. (A) Time-lapse images depicting the engulfment process of C3 and C1 (arrows) in wild-type and *dyn-1* mutant embryos. Embryos all express *P_{ced-1} gfp::rab-5*. 0 min, time point when the two ventral hypodermal cells ABplaapppp and ABpraapppp contact each other at the embryonic midline. Bars, 2 μ m. Extended pseudopods are marked by arrowheads. (a–e) Engulfment process of cell corpse C3 in a wild-type embryo. (f–j) Example of an abortive attempt of pseudopod extension (arrowhead) in a *dyn-1(en9)* embryo. (f–j) DIC images showing the position of the cell corpse C3. (k–o) GFP images correspond to f–j, respectively, which show normally initiated (n, arrowhead) yet failed pseudopod extension from the supposed-to-be engulfing cell ABplaapppp during the recording period. (p–v) Example of prolonged pseudopod extension around the C1 cell corpse in a *dyn-1(en40)* embryo. (w) A diagram depicting the physical contact between the two extending hypodermal cells at the ventral midline at the 0-min time point, which is the reference point for measuring the timing of the initiation of pseudopod extension. (B and C) The frequency of each type of engulfment defects observed from *dyn-1(en9)* or *dyn-1(en40)* embryos measured using GFP::RAB-5 (B) or CED-1C::GFP (C) as a reporter, respectively. The initiation time of pseudopod extension was measured using the time point that ABplaapppp and ABpraapppp made contact as the 0-min time point. The time between the initiation of pseudopod extension and the closure of a phagocytic cup is defined as the duration of pseudopod extension. All data were obtained from observations of the engulfment of C1, C2 and C3. n, total number of engulfment events scored.

A

Property	DYN-1(I401F)	DYN-1(G40E)
Allele name	<i>en9</i>	<i>en40</i>
GTP-binding	Normal	Inactive
GTP hydrolysis, basal activity	Normal	Inactive
GTP hydrolysis, lipid-induced activity	Inactive	Inactive
Self-assembly, <i>in vitro</i>	Inactive	Normal
Self-assembly, <i>in vivo</i>	Defective	Normal
Dominant-negative effect	No	Yes
Suppression of dominant-negative effect	Yes	NA
Association with target membranes	Severely defective	Normal
Dissociation from target membranes	NA	Severely defective
Recruitment of RAB-5	Severely defective	Severely defective
Recruitment of RAB-7	Severely defective	Relatively normal
Phagosome maturation	Severely defective	Severely defective
Engulfment	Defective, less penetrating	Defective

B

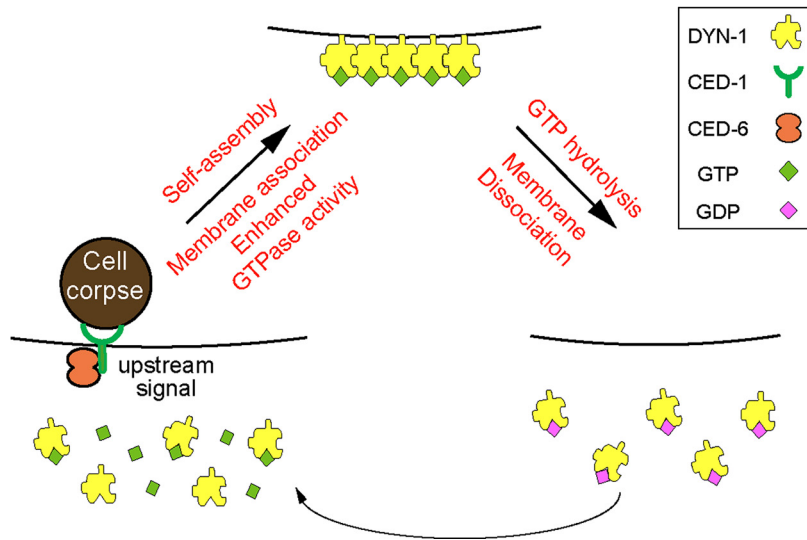


Figure 11. Models depicting the molecular mechanisms that regulate the function of DYN-1 during the removal of apoptotic cells. (A) Table comparing the biochemical properties and functional defects of the mutant DYN-1 defective in self-assembly or GTP binding. NA, not applicable. (B) Model proposing an autoregulatory loop that regulates the temporal association of DYN-1 to its target membrane. In response to an upstream recruitment signal, DYN-1 molecules undergo self-assembly, an event that enables DYN-1 to associate with target membrane. Meanwhile, self-assembly enhances the GTP hydrolysis activity of DYN-1, which results in the disassembly of DYN-1 oligomers and the consequential dissociation of DYN-1 from its target membrane. In the continuing presence of the upstream signal, DYN-1 monomers will again assemble along the membrane surface. As a consequence, the apparently opposite effects of self-assembly and GTP hydrolysis reach a balance and together, they maintain a steady-state level of DYN-1 on the target membrane. Once the upstream signal disappears, the high-level GTPase activity of DYN-1 oligomers allows rapid dissociation of DYN-1 from the target membrane.

membrane localization of dynamin, it was found that the PH domain alone was insufficient to specify DYN-1's localization (Labrousse *et al.*, 1998). *In vitro*, the lipid binding affinity of dynamin's PH domain monomers seems weak but is significantly enhanced when the PH domain is oligomerized (Kavran *et al.*, 1998; Klein *et al.*, 1998). Among other possibilities, self-assembly may induce a conformational change and enhance dynamin's affinity for membrane lipids. Our work reported here indicates that *in vivo*, as observed *in vitro* in cryo-EM studies, dynamin oligomers display a higher affinity for membranes than monomers. By this means, self-assembly strengthens the association of dynamin with its target regions on the plasma and intracellular membranes. As upstream regulators of DYN-1, the phago-

cytic receptor CED-1 and its adaptor CED-6 could recruit DYN-1 to the region of action by promoting either the self-assembly of DYN-1 monomers, or the association DYN-1 oligomers with specific membrane lipids such as phosphatidylinositol 4,5-bisphosphate, or both (Figure 11B).

In contrast to the effect of the I401F mutation, we found that abolishing the GTP binding and hence the GTPase activity of endogenous DYN-1 via the G40E mutation did not affect DYN-1's self-assembly or its ability to associate with its target membranes *in vivo* (Figure 11A). Rather, both *in vitro* and *in vivo*, DYN-1(G40E) mutant protein failed to disappear from its target membranes, indicating a defect in the disassembly of DYN-1 oligomers or the subsequent dissociation of monomers from target membranes. DYN-1's GTP hy-

drololysis and self-assembly activities thus contribute opposite effects toward DYN-1's association to target membranes.

We propose that these two opposite effects together establish an autoregulatory loop that precisely controls the duration and steady-state level of DYN-1 on its target membranes (Figure 11B). According to this model, in response to an upstream signal, DYN-1 molecules undergo self-assembly, an event that leads it to associate with target membranes. Meanwhile, self-assembly enhances the GTP hydrolysis activity of DYN-1, which subsequently results in the disassembly of DYN-1 oligomers and the consequential dissociation of DYN-1 molecules from its target membranes, a process akin to ATP or GTP hydrolysis in actin and tubulin polymerization, respectively (Desai and Mitchison, 1997). As long as the upstream signal is present, DYN-1 monomers will once again assemble along the membrane surface. As a consequence, the cycle of DYN-1 association to and dissociation from target membranes reach equilibrium and maintain a dynamic, steady state level of DYN-1 on the target membranes. Once the upstream signal disappears, the assembly-enhanced GTPase activity of DYN-1 oligomers enables rapid dissociation of DYN-1 from target membranes, as observed from phagosome surfaces (Figures 7F and 11B).

The dissociation of DYN-1 from its target membranes also plays an indirect, yet important role in the timely association of DYN-1 to pseudopods and phagosomes. As an essential factor for many vesicle trafficking events, DYN-1 is targeted to the plasma membrane and intracellular membranes of different identities (Hinshaw, 2000; Praefcke and McMahon, 2004). In engulfing cells, DYN-1(G40E)::GFP, whose membrane dissociation function is impaired, was heavily aggregated to cytoplasmic puncta, which were presumed intracellular vesicles; furthermore, the association of DYN-1(G40E) to pseudopods or phagosomes was significantly delayed in relation to the timing of engulfment. This delay could be a result of the delayed dissociation of DYN-1(G40E) from other cellular compartments and is likely to further affect DYN-1's function in promoting pseudopod extension and phagosome maturation.

Self-Assembly, GTP Hydrolysis, and DYN-1's Functions in Phagosome Maturation

Both self-assembly and GTPase mutations in DYN-1 cause severe defects in phagosome maturation. Previously, we have established that DYN-1 mediates the fusion of early endosomes and lysosomes to phagosomes (Yu *et al.*, 2006, 2008). To understand the functional relationship of DYN-1's self-assembly and GTP binding activities with the fusion of intracellular organelles to phagosomes, we examined events that control these fusion events. In particular, we observed common and differential effects of self-assembly and GTP binding mutations toward the phagosomal recruitment of two membrane tethering factors RAB-5 and RAB-7, which are essential for the specific association of early endosomes and lysosomes to phagosomes, respectively (Figure 11B; Vieira *et al.*, 2002; Harrison *et al.*, 2003; Yu *et al.*, 2008).

We determined the precise temporal pattern for the enrichment of both RAB-5 and RAB-7 on phagosomal surfaces in wild-type embryos (Figures 7E and 9; Yu *et al.*, 2008). We further found that both the self-assembly and GTP binding mutations cause substantial delay of RAB-5 recruitment to phagosomes to various degrees, indicating that the oligomerization and GTP binding of DYN-1 are both required for the timely recruitment of RAB-5, and further suggesting that the DYN-1 molecules that are capable of recruiting RAB-5 are in a polymer state localized to the surface of phagosomes and likely to be in a GTP-bound form.

In contrast, whereas the self-assembly mutation of DYN-1 nearly completely destroys the temporal recruitment pattern of RAB-7 to phagosomes, the GTP binding mutation only causes a weak and partially penetrating delay of RAB-7 recruitment. These differential effects indicate that the self-assembly and the consequential phagosomal association of DYN-1 is both necessary and sufficient for the recruitment of RAB-7 to phagosomes, whereas the GTP binding ability does not seem to make a significant contribution to this event. To our knowledge, this is the first report of these types of differential effects related to the *in vivo* functions of dynamin, which suggests that novel and differential molecular mechanisms are involved in dynamin-mediated recruitment of RAB-5 and RAB-7. Perhaps RAB-5 or its associating protein complex selectively interacts with the GTP-bound form of DYN-1, whereas the RAB-7 complex does not distinguish between GTP- or GDP-bound forms of DYN-1.

In wild-type embryos, RAB-5 precedes RAB-7 for associating with phagosomal surfaces (Figure 7E). In the *dyn-1(en40)* mutant background, however, many phagosomes that are labeled with enriched GFP::RAB-7 signal have not been labeled with GFP::RAB-5 yet, indicating that the DYN-1 mediated recruitment of RAB-5 and RAB-7 might be independent of each other. Further study of the molecular mechanisms behind the phagosomal recruitment of RAB-5 and RAB-7 will further reveal the exact roles of DYN-1 in these events.

The tight correlation between the defects in RAB-5 and RAB-7 recruitment and maintenance and the defects in phagosome maturation observed in the *dyn-1(en9)* mutant embryos reveals that the failure to recruit RAB-5 and RAB-7 to phagosomes is probably the major cause for the severely delayed or blocked phagosome degradation. In *dyn-1(en40)* mutant embryos, the strong phagosome maturation defect is also well correlated with the defect in recruiting RAB-5. In contrast, we found that overexpression of a functional GFP::RAB-7 from an extrachromosomal array, which possesses the full rescuing capacity of defects displayed by *rab-7* null mutants (Yu *et al.*, 2008), partially suppressed the delay of phagosome maturation in *dyn-1(en40)* mutants. This suppression activity is consistent with the observation that the G40E mutation does not significantly affect the recruitment of RAB-7 to phagosomal surfaces, and further suggests that in *dyn-1(en40)* mutants, as long as RAB-7 is associated with the phagosomal membranes, it is functional in promoting phagosome maturation. The mechanism behind the suppression effect awaits investigation. It is possible that in engulfing cells, the endogenous RAB-7 molecules are limited in number. Once overexpressed from the transgenic array, the excessive amount of RAB-7 molecules might result in the recruitment of an excessive amount of lysosomes to phagosomes, which might compensate for the lack of early endosome incorporation to phagosomes due to the lack of RAB-5 association with phagosomes in *dyn-1(en40)* mutants.

In summary, our current observations, together with previous studies, indicate that DYN-1 directly promotes phagosome maturation by acting on the surface of phagosomes. Furthermore, DYN-1 promotes membrane fusion primarily through controlling the recruitment of membrane tethering factors. The self-assembly and GTP binding activities of DYN-1 contribute to common and different aspects of this fusion-promoting activity. In addition, recent studies have shown that the association of dynamin polymers with membrane stabilizes membranes of high curvature (Bashkirov *et al.*, 2008). The disassembly of dynamin helix promotes membrane fission (Bashkirov *et al.*, 2008; Pucadyil and Schmid, 2008). In addition to recruiting tethering factors, DYN-1 may

also act in remodeling phagosomal membranes during phagosome maturation.

During engulfment, the GTP binding and self-assembly activities also play roles for DYN-1's function in promoting pseudopod initiation and extension. The GTP-bound form of DYN-1 on engulfing cell membranes might be critical for recruiting intracellular vesicle to pseudopods. Alternatively, the membrane fission activity of DYN-1, which requires GTP hydrolysis, might act on the surface of intracellular membranes to generate sufficient amount of intracellular vesicles for fusion with pseudopods.

Given that classical dynamins possess highly conserved domain structure and amino acid sequence from *C. elegans* to humans, and that human dynamin 2 can partially replace the function of DYN-1 in *C. elegans* (Clark *et al.*, 1997; Yu *et al.*, 2006), the mechanisms underlying the functions of dynamins are likely to be conserved from *C. elegans* to humans. Our findings in *C. elegans* will shed lights on the mechanism of mammalian dynamins in the removal of apoptotic cells and other biological processes.

ACKNOWLEDGMENTS

We thank C.-D. Hu for BiFC vectors; T. Wensel for help with the GTP binding assay; X. He for the DeltaVision microscope; X. He, C. Peters, and members of the Z. Z. laboratory for helpful comments. Support for Z. Z. includes National Institutes of Health grant GM-067848, the Cancer Research Institute, and the Rita Allen Foundation. D. D. acknowledges the Israel Science Foundation, the Charles H. Revson Foundation (grant 530/03), and Russell Berrie Nanotechnology Institute at the Technion for financial support. F.A.Q. acknowledges support from NIH (GM088803) and the Welch Foundation (Q581).

REFERENCES

Bashkurov, P. V., Akimov, S. A., Evseev, A. I., Schmid, S. L., Zimmerberg, J., and Frolov, V. A. (2008). GTPase cycle of dynamin is coupled to membrane squeeze and release, leading to spontaneous fission. *Cell* 135, 1276–1286.

Bloom, L., and Horvitz, H. R. (1997). The *Caenorhabditis elegans* gene *unc-76* and its human homologs define a new gene family involved in axonal outgrowth and fasciculation. *Proc. Natl. Acad. Sci. USA* 94, 3414–3419.

Brenner, S. (1974). The genetics of *Caenorhabditis elegans*. *Genetics* 77, 71–94.

Cai, H., Reinisch, K., and Ferro-Novick, S. (2007). Coats, tethers, Rabs, and SNAREs work together to mediate the intracellular destination of a transport vesicle. *Dev. Cell* 12, 671–682.

Clark, S. G., Shurland, D. L., Meyerowitz, E. M., Bargmann, C. I., and van der Bliek, A. M. (1997). A dynamin GTPase mutation causes a rapid and reversible temperature-inducible locomotion defect in *C. elegans*. *Proc. Natl. Acad. Sci. USA* 94, 10438–10443.

Collins, C. A., and Vallee, R. B. (1986). A microtubule-activated ATPase from sea urchin eggs, distinct from cytoplasmic dynein and kinesin. *Proc. Natl. Acad. Sci. USA* 83, 4799–4803.

Danino, D., Bernheim-Groswasser, A., and Talmon, Y. (2001). Digital cryogenic transmission electron microscopy: an advanced tool for direct imaging of complex fluids colloids and surfaces. *Physicochem. Eng. Asp.* 183–185, 113–122.

Danino, D., Moon, K. H., and Hinshaw, J. E. (2004). Rapid constriction of lipid bilayers by the mechanochemical enzyme dynamin. *J. Struct. Biol.* 147, 259–267.

Dawson, J. C., Legg, J. A., and Machesky, L. M. (2006). Bar domain proteins: a role in tubulation, scission and actin assembly in clathrin-mediated endocytosis. *Trends Cell Biol.* 16, 493–498.

Desai, A., and Mitchison, T. J. (1997). Microtubule polymerization dynamics. *Annu. Rev. Cell. Dev. Biol.* 13, 83–117.

Di, A., Nelson, D. J., Bindokas, V., Brown, M. E., Libunao, F., and Palfrey, H. C. (2003). Dynamin regulates focal exocytosis in phagocytosing macrophages. *Mol. Biol. Cell* 14, 2016–2028.

Evergren, E., Tomilin, N., Vasylieva, E., Sergeeva, V., Bloom, O., Gad, H., Capani, F., and Shupliakov, O. (2004). A pre-embedding immunogold approach for detection of synaptic endocytic proteins in situ. *J. Neurosci. Methods* 135, 169–174.

Gold, E. S., Underhill, D. M., Morrisette, N. S., Guo, J., McNiven, M. A., and Aderem, A. (1999). Dynamin 2 is required for phagocytosis in macrophages. *J. Exp. Med.* 190, 1849–1856.

Grant, B., and Hirsh, D. (1999). Receptor-mediated endocytosis in the *Caenorhabditis elegans* oocyte. *Mol. Biol. Cell* 10, 4311–4326.

Harrison, R. E., Bucci, C., Vieira, O. V., Schroer, T. A., and Grinstein, S. (2003). Phagosomes fuse with late endosomes and/or lysosomes by extension of membrane protrusions along microtubules: role of Rab7 and RILP. *Mol. Cell Biol.* 23, 6494–6506.

Hiatt, S. M., Shyu, Y. J., Duren, H. M., and Hu, C. D. (2008). Bimolecular fluorescence complementation (BiFC) analysis of protein interactions in *Caenorhabditis elegans*. *Methods* 45, 185–191.

Hinshaw, J. E. (2000). Dynamin and its role in membrane fission. *Annu. Rev. Cell. Dev. Biol.* 16, 483–519.

Hinshaw, J. E., and Schmid, S. L. (1995). Dynamin self-assembles into rings suggesting a mechanism for coated vesicle budding. *Nature* 374, 190–192.

Hoppins, S., and Nunnari, J. (2009). The molecular mechanism of mitochondrial fusion. *Biochim. Biophys. Acta* 1793, 20–26.

Hu, C. D., Chinenov, Y., and Kerppola, T. K. (2002). Visualization of interactions among bZIP and Rel family proteins in living cells using bimolecular fluorescence complementation. *Mol. Cell* 9, 789–798.

Jin, Y. (1999). Transformation. In: *C. elegans*, a Practical Approach, ed. I. A. Hope, Oxford, United Kingdom: Oxford University Press, 69–96.

Kavran, J. M., Klein, D. E., Lee, A., Falasca, M., Isakoff, S. J., Skolnik, E. Y., and Lemmon, M. A. (1998). Specificity and promiscuity in phosphoinositide binding by pleckstrin homology domains. *J. Biol. Chem.* 273, 30497–30508.

Kelly, W. G., Xu, S., Montgomery, M. K., and Fire, A. (1997). Distinct requirements for somatic and germline expression of a generally expressed *Caenorhabditis elegans* gene. *Genetics* 146, 227–238.

Kerppola, T. K. (2006). Design and implementation of bimolecular fluorescence complementation (BiFC) assays for the visualization of protein interactions in living cells. *Nat. Protoc.* 1, 1278–1286.

Kinchen, J. M., Doukoumetzidis, K., Almendinger, J., Stergiou, L., Tosello-Tramont, A., Sifri, C. D., Hengartner, M. O., and Ravichandran, K. S. (2008). A pathway for phagosome maturation during engulfment of apoptotic cells. *Nat. Cell Biol.* 10, 556–566.

Kinchen, J. M., and Ravichandran, K. S. (2008). Phagosome maturation: going through the acid test. *Nat. Rev. Mol. Cell Biol.* 9, 781–795.

Kitano, M., Nakaya, M., Nakamura, T., Nagata, S., and Matsuda, M. (2008). Imaging of Rab5 activity identifies essential regulators for phagosome maturation. *Nature* 453, 241–245.

Klein, D. E., Lee, A., Frank, D. W., Marks, M. S., and Lemmon, M. A. (1998). The pleckstrin homology domains of dynamin isoforms require oligomerization for high affinity phosphoinositide binding. *J. Biol. Chem.* 273, 27725–27733.

Konikoff, F. M., Danino, D., Weihs, D., Rubin, M., and Talmon, Y. (2000). Microstructural evolution of lipid aggregates in nucleating model and human bile visualized by cryogenic transmission electron microscopy. *Hepatology* 31, 261–268.

Labrousse, A. M., Shurland, D. L., and van der Bliek, A. M. (1998). Contribution of the GTPase domain to the subcellular localization of dynamin in the nematode *Caenorhabditis elegans*. *Mol. Biol. Cell* 9, 3227–3239.

Lu, N., Yu, X., He, X., and Zhou, Z. (2009). Detecting apoptotic cells and monitoring their clearance in the nematode *Caenorhabditis elegans*. *Methods Mol. Biol.* 559, 357–370.

Metzstein, M. M., Stanfield, G. M., and Horvitz, H. R. (1998). Genetics of programmed cell death in *C. elegans*: past, present and future. *Trends Genet.* 14, 410–416.

Nagai, T., Iyata, K., Park, E. S., Kubota, M., Mikoshiba, K., and Miyawaki, A. (2002). A variant of yellow fluorescent protein with fast and efficient maturation for cell-biological applications. *Nat. Biotechnol.* 20, 87–90.

Narayanan, R., Leonard, M., Song, B. D., Schmid, S. L., and Ramaswami, M. (2005). An internal GAP domain negatively regulates presynaptic dynamin in vivo: a two-step model for dynamin function. *J. Cell Biol.* 169, 117–126.

Niemann, H. H., Knetsch, M. L., Scherer, A., Manstein, D. J., and Kull, F. J. (2001). Crystal structure of a dynamin GTPase domain in both nucleotide-free and GDP-bound forms. *EMBO J.* 20, 5813–5821.

Orth, J. D., and McNiven, M. A. (2003). Dynamin at the actin-membrane interface. *Curr. Opin. Cell Biol.* 15, 31–39.

Peters, C., Baars, T. L., Buhler, S., and Mayer, A. (2004). Mutual control of membrane fission and fusion proteins. *Cell* 119, 667–678.

- Praefcke, G. J., and McMahon, H. T. (2004). The dynamin superfamily: universal membrane tubulation and fission molecules? *Nat. Rev. Mol. Cell Biol.* 5, 133–147.
- Pucadyil, T. J., and Schmid, S. L. (2008). Real-time visualization of dynamin-catalyzed membrane fission and vesicle release. *Cell* 135, 1263–1275.
- Ramachandran, R., Surka, M., Chappie, J. S., Fowler, D. M., Foss, T. R., Song, B. D., and Schmid, S. L. (2007). The dynamin middle domain is critical for tetramerization and higher-order self-assembly. *EMBO J.* 26, 559–566.
- Riddle, D. L., Blumenthal, T., Meyer, B. J., and Priess, J. R. (eds.) (1997). *C. elegans II*, Plainview, NY: Cold Spring Harbor Laboratory Press.
- Salim, K., *et al.* (1996). Distinct specificity in the recognition of phosphoinositides by the pleckstrin homology domains of dynamin and Bruton's tyrosine kinase. *EMBO J* 15, 6241–6250.
- Savill, J., and Fadok, V. (2000). Corpse clearance defines the meaning of cell death. *Nature* 407, 784–788.
- Schmid, S. L., McNiven, M. A., and De Camilli, P. (1998). Dynamin and its partners: a progress report. *Curr. Opin. Cell Biol.* 10, 504–512.
- Sever, S., Muhlberg, A. B., and Schmid, S. L. (1999). Impairment of dynamin's GAP domain stimulates receptor-mediated endocytosis. *Nature* 398, 481–486.
- Shyu, Y. J., Hiatt, S. M., Duren, H. M., Ellis, R. E., Kerppola, T. K., and Hu, C. D. (2008). Visualization of protein interactions in living *Caenorhabditis elegans* using bimolecular fluorescence complementation analysis. *Nat. Protoc.* 3, 588–596.
- Song, B. D., Leonard, M., and Schmid, S. L. (2004). Dynamin GTPase domain mutants that differentially affect GTP binding, GTP hydrolysis, and clathrin-mediated endocytosis. *J. Biol. Chem.* 279, 40431–40436.
- Stowell, M. H., Marks, B., Wigge, P., and McMahon, H. T. (1999). Nucleotide-dependent conformational changes in dynamin: evidence for a mechanical molecular spring. *Nat. Cell Biol.* 1, 27–32.
- Stringham, E. G., Dixon, D. K., Jones, D., and Candido, E. P. (1992). Temporal and spatial expression patterns of the small heat shock (hsp16) genes in transgenic *Caenorhabditis elegans*. *Mol. Biol. Cell* 3, 221–233.
- Sulston, J. E., and Horvitz, H. R. (1977). Post-embryonic cell lineages of the nematode, *Caenorhabditis elegans*. *Dev. Biol.* 56, 110–156.
- Sulston, J. E., Schierenberg, E., White, J. G., and Thomson, N. (1983). The embryonic cell lineage of the nematode *Caenorhabditis elegans*. *Dev. Biol.* 100, 64–119.
- Sweitzer, S. M., and Hinshaw, J. E. (1998). Dynamin undergoes a GTP-dependent conformational change causing vesiculation. *Cell* 93, 1021–1029.
- Szafer, E., Rotman, M., and Cassel, D. (2001). Regulation of GTP hydrolysis on ADP-ribosylation factor-1 at the Golgi membrane. *J. Biol. Chem.* 276, 47834–47839.
- Takei, K., Haucke, V., Slepnev, V., Farsad, K., Salazar, M., Chen, H., and De Camilli, P. (1998). Generation of coated intermediates of clathrin-mediated endocytosis on protein-free liposomes. *Cell* 94, 131–141.
- Takei, K., McPherson, P. S., Schmid, S. L., and De Camilli, P. (1995). Tubular membrane invaginations coated by dynamin rings are induced by GTP-gamma S in nerve terminals. *Nature* 374, 186–190.
- Touret, N., *et al.* (2005). Quantitative and dynamic assessment of the contribution of the ER to phagosome formation. *Cell* 123, 157–170.
- Vieira, O. V., Botelho, R. J., and Grinstein, S. (2002). Phagosome maturation: aging gracefully. *Biochem. J.* 366, 689–704.
- Warnock, D. E., Hinshaw, J. E., and Schmid, S. L. (1996). Dynamin self-assembly stimulates its GTPase activity. *J. Biol. Chem.* 271, 22310–22314.
- Yu, X., Lu, N., and Zhou, Z. (2008). Phagocytic receptor CED-1 initiates a signaling pathway for degrading engulfed apoptotic cells. *PLoS Biol.* 6, e61.
- Yu, X., Odera, S., Chuang, C. H., Lu, N., and Zhou, Z. (2006). *C. elegans* Dynamin mediates the signaling of phagocytic receptor CED-1 for the engulfment and degradation of apoptotic cells. *Dev. Cell* 10, 743–757.
- Zheng, J., Cahill, S. M., Lemmon, M. A., Fushman, D., Schlessinger, J., and Cowburn, D. (1996). Identification of the binding site for acidic phospholipids on the pH domain of dynamin: implications for stimulation of GTPase activity. *J. Mol. Biol.* 255, 14–21.
- Zhou, Z., Hartwig, E., and Horvitz, H. R. (2001b). CED-1 is a transmembrane receptor that mediates cell corpse engulfment in *C. elegans*. *Cell* 104, 43–56.
- Zhou, Z., and Yu, X. (2008). Phagosome maturation during the removal of apoptotic cells: receptors lead the way. *Trends Cell Biol.* 18, 474–485.